Carbon Nanostructures

I. Graphene

Outline:

- Introduction (Making graphene, Applications, etc.)
- Band structure
- Physics of Dirac electrons (Barry phase, Klein tunneling)
- Half-Integer Quantum Hall Effect
- Mobility in Graphene

References:

- C. Beenakker, Reviews of Modern Physics, 80, 1337 (2008)
- A. Geim talk, TNT Conference, 2010 http://www.tntconf.org/2010/Presentaciones/TNT2010_Geim.pdf
- A. Geim, Nobel lecture, 2010 http://www.nobelprize.org/nobel_prizes/physics/laureates/2010/geim-lecture-slides.pdf
- F. Bonaccorso et al., NATURE PHOTONICS 4, 611 (2010)
- E. McCann Graphene monolayers Lancaster University, UK Tight-binding model, QHE
- L. Tapaszto & J. Cserti talks, MAFIHE Teli Iskola a Grafenrol 2011, ELTE

Carbon nanostructures

Fullerene
0D

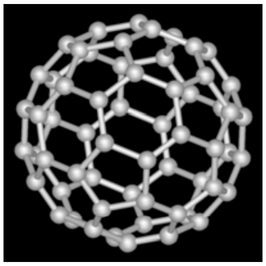

1985
H.W.Kroto
Mass spectrometer

Nanotube
1D

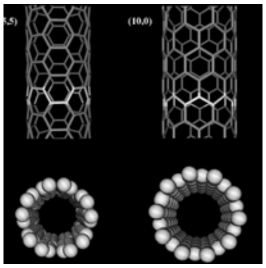

1991
S Iijima
Electron microscope

Graphene
2D

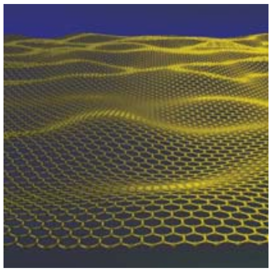

2004
K. S. Novoselov
Optical microscope

Graphene – Nobel Prize in Physics 2010

Andre Geim Kostya Novoselov

Electric Field Effect in Atomically Thin Carbon Films

K. S. Novoselov,[1] A. K. Geim,[1*] S. V. Morozov,[2] D. Jiang,[1] Y. Zhang,[1] S. V. Dubonos,[2] I. V. Grigorieva,[1] A. A. Firsov[2]

We describe monocrystalline graphitic films, which are a few atoms thick but are nonetheless stable under ambient conditions, metallic, and of remarkably high quality. The films are found to be a two-dimensional semimetal with a tiny overlap between valence and conductance bands, and they exhibit a strong ambipolar electric field effect such that electrons and holes in concentrations up to 10^{13} per square centimeter and with room-temperature mobilities of ~10,000 square centimeters per volt-second can be induced by applying gate voltage.

22 OCTOBER 2004 VOL 306 SCIENCE www.sciencemag.org

"for groundbreaking experiments regarding the two dimensional material graphene"

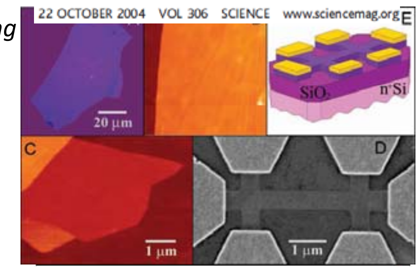

Surprising, since growth of macroscopic 2D objects is strictly forbidden due to phonons (Mermin Wagner)

a) Mechanical exfoliation

+

Manchester, Science 2004; PNAS 2005

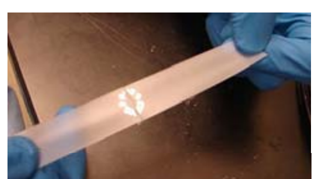

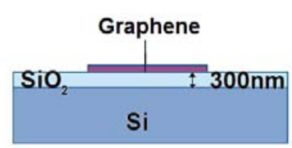

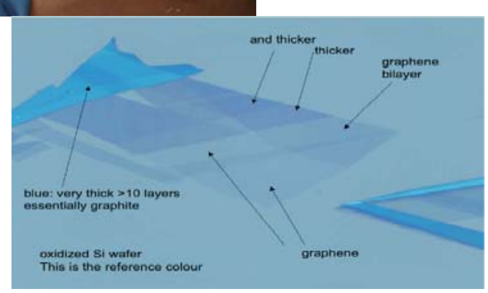

For proper SiO2 thickness interference makes it visible by optical microscope
+ Even size of 1mm, + high quality, - low yield

b) Mechanical or Chemical extraction

sonication + centrifugation, often intercalation

→ Submicrometer crystallites
+ Mass production, industrial scale
- Small falke size
-Remaining attached chemicals (oxide)
→ Good for polycrystalline films and composite materials. Suspension can be printed resulting highly conductive bendable film

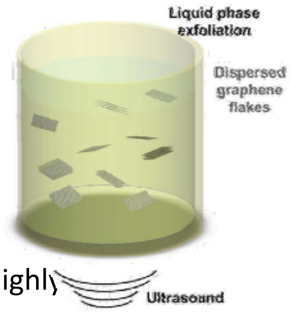

Ruoff, Nature 2006, Manchester, Nanolett '08,Coleman et al, Nature Nano '08

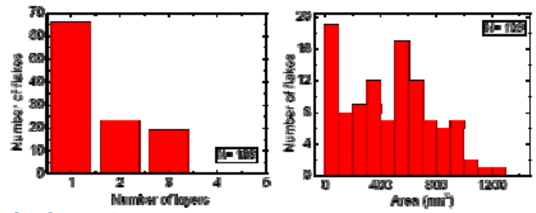

http://www.vorbeck.com/

b) Epitaxial growth of a monolayer

Grow a monolayer of C and chemically remove the substrate

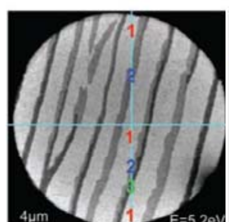

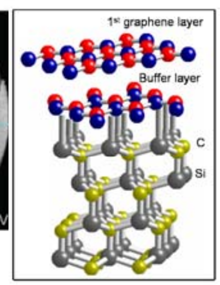

1) SiC substrate: (upper figs.)
SiC is insulator, Graphene layers grow as a carpet on the surface. Layers are electrically well isolated (different stacking). Possible to grow 1,2 layers.
- Difficult growth process

2) CVD on Cu, Ni (Lower figs.) "Easy" to do: T + gas flow. Self terminating process. Result: single layer, - polycrystalline, it follows the crystallites of the metal surface, Use HCl to remove substrate. (commercial available)

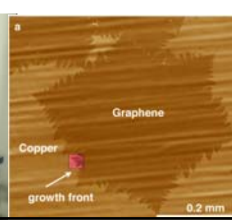

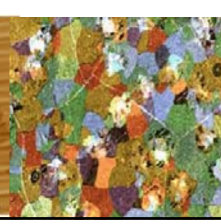

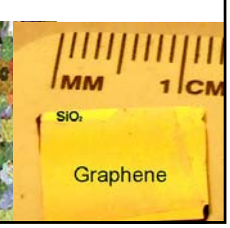

Identification

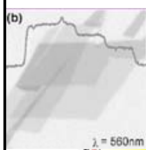

Optically *Contrast of graphene at diff. SiO_2 thickness.*

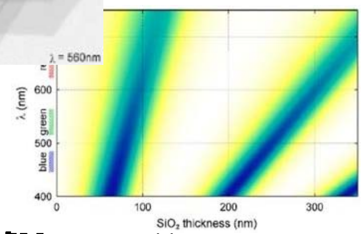

Raman spectroscopy *measure the energy difference of reflected laser light*
e.g. layer thickness can be determined from the 2D peak

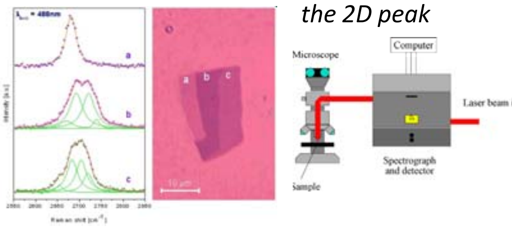

AFM *e.g. possible to determine thickness*

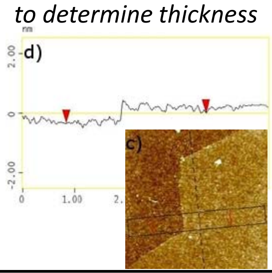

STM *e.g. exfoliated on metal substrate*

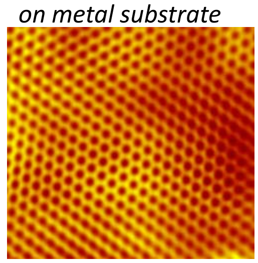

TEM *e.g. crystalite boarder SiC*

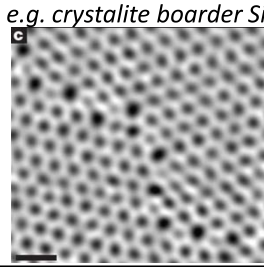

Properties

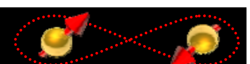

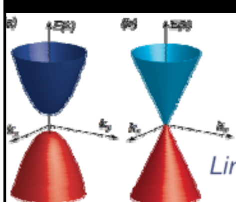

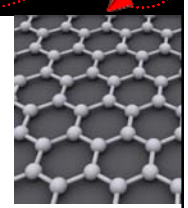

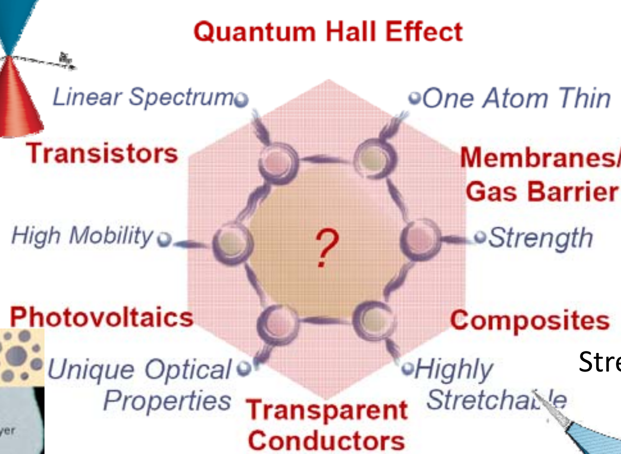

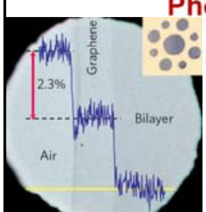

R_m=42N/m
Stretchable 20%

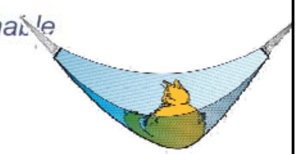

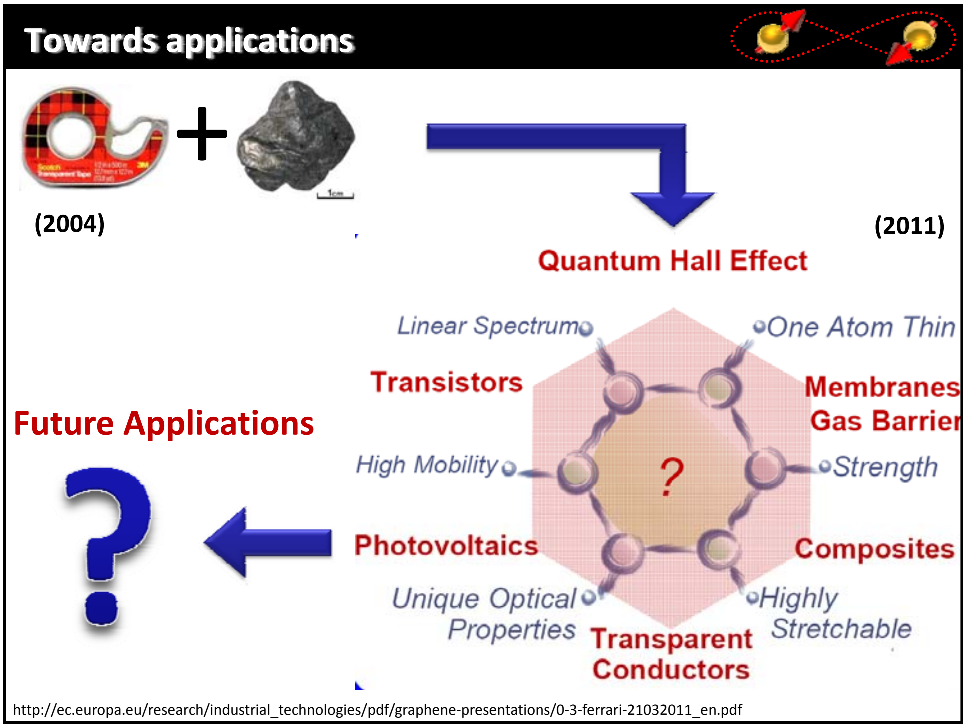
Towards applications
(2004)
(2011)
Quantum Hall Effect
Linear Spectrum
One Atom Thin
Transistors
Membranes
Gas Barrier
Future Applications
High Mobility
?
Strength
Photovoltaics
Composites
Unique Optical Properties
Highly Stretchable
Transparent Conductors
?
http://ec.europa.eu/research/industrial_technologies/pdf/graphene-presentations/0-3-ferrari-21032011_en.pdf

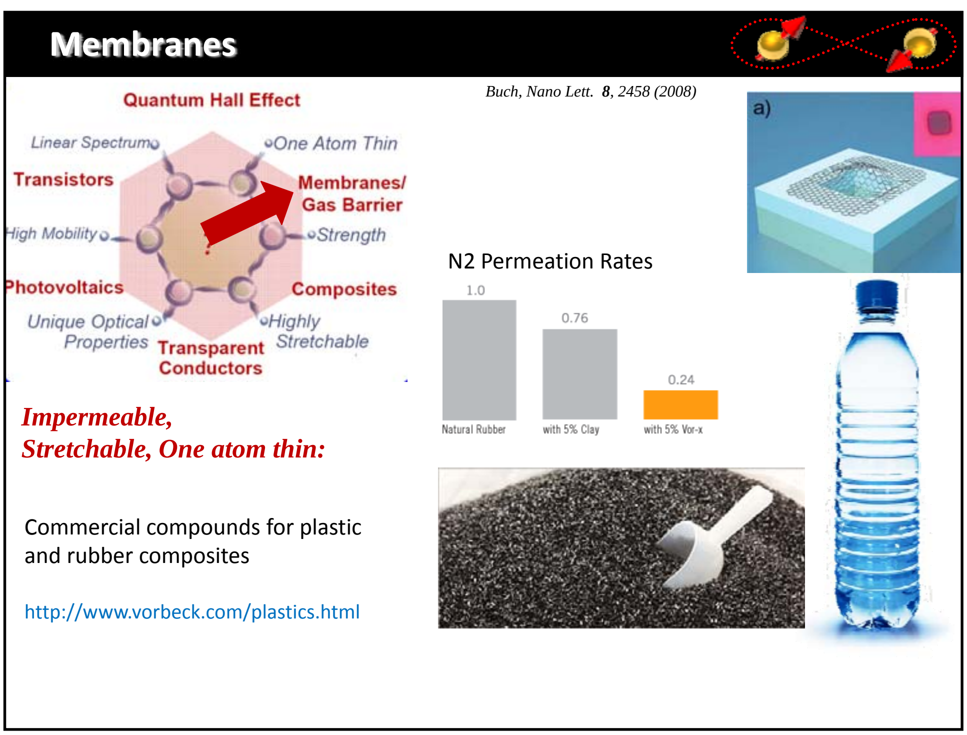
Membranes
Quantum Hall Effect
Linear Spectrum
One Atom Thin
Transistors
Membranes/
Gas Barrier
High Mobility
Strength
Photovoltaics
Composites
Unique Optical Properties
Highly Stretchable
Transparent Conductors
Buch, Nano Lett. 8, 2458 (2008)
a)
N2 Permeation Rates
1.0
0.76
0.24
Natural Rubber
with 5% Clay
with 5% Vor-x
Impermeable,
Stretchable, One atom thin:
Commercial compounds for plastic and rubber composites
http://www.vorbeck.com/plastics.html

Composites

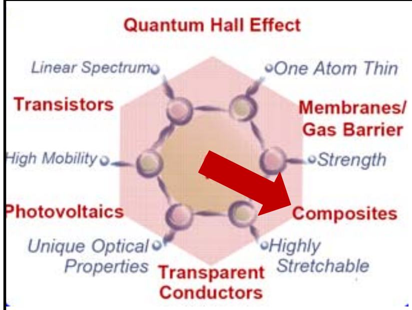

Light, stretchable, strong:

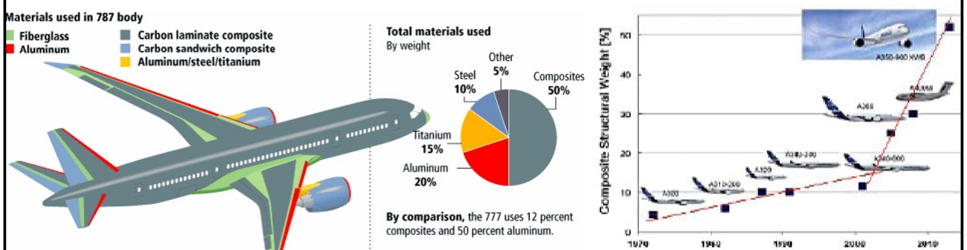

http://ec.europa.eu/research/industrial_technologies/pdf/graphene-presentations/0-3-ferrari-21032011_en.pdf

Optoelectronics

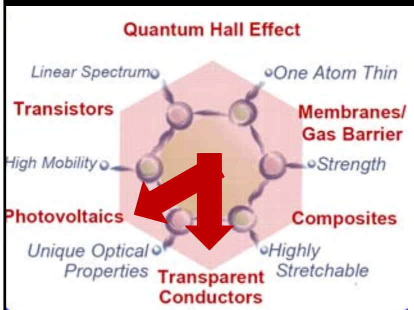

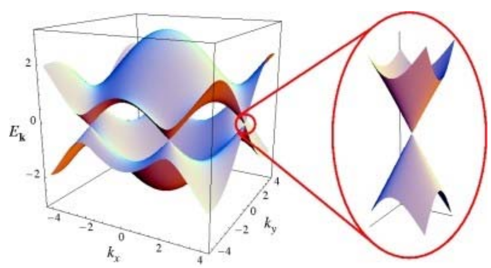

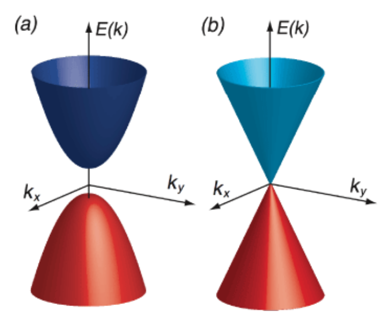

Bonaccorso et al. Nature Photonics 4, 611 (2010)

Optoelectronics

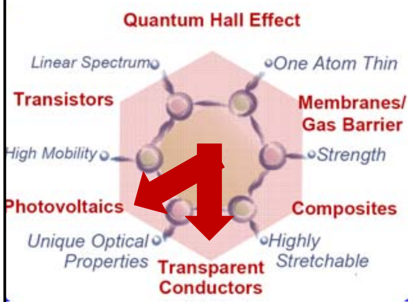

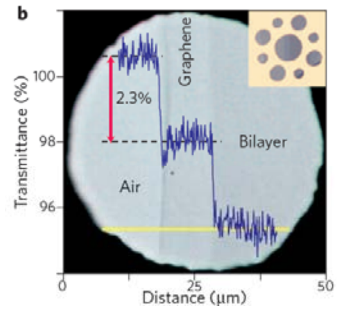

One atom thin:
- Transmittance is high, 97.7%

Linear spectrum:
- For any excitation there is e-h pair

→Broad band applications

-Pair carrier collision (fast relaxation) can not lead to interband relaxation → Pauli blocking

→ Saturable absorption

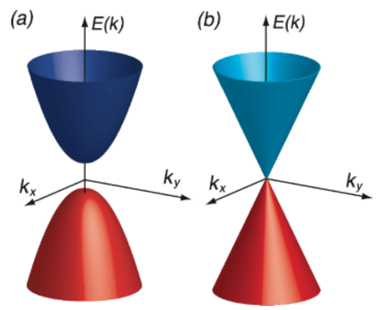

Bonaccorso et al. Nature Photonics 4, 611 (2010)

Optoelectronics

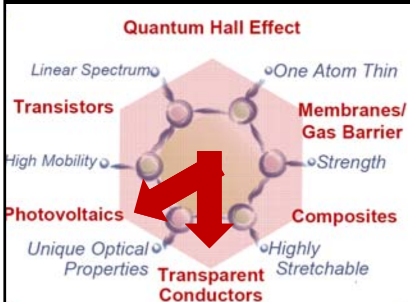

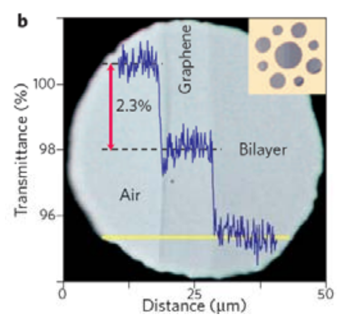

One atom thin:
- Transmittance is high, 97.7%

Linear spectrum:
- For any excitation there is e-h pair

→Broad band applications

-Pair carrier collision (fast relaxation) can not lead to interband relaxation → Pauli blocking

→ Saturable absorption

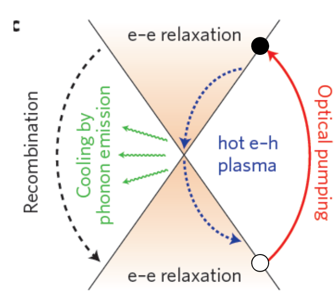

Bonaccorso et al. Nature Photonics 4, 611 (2010)

Optoelectronics

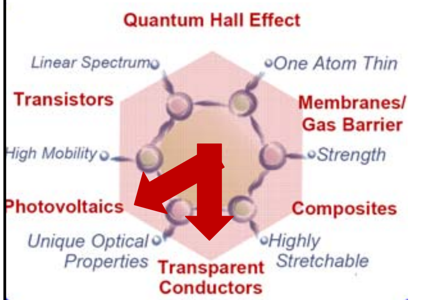

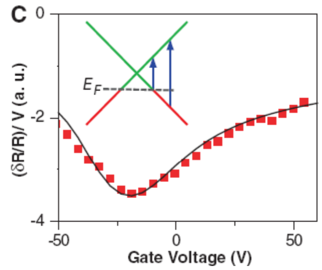

Wang ,Science 320, 206 (2008)

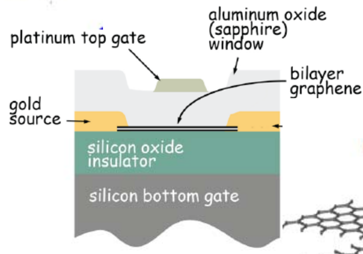

Bilayer + E

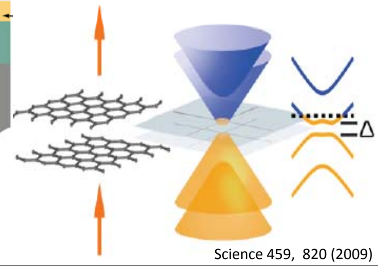

Low e density,
gate tunable E_F:
Tunable gap up to 0.25eV
in bilayer graphene
→Far infrared light generation, amplification, detection

Modifications of Graphene:
e.g. Grapheneoxide show broad photo luminescence

Science 459, 820 (2009)

Transparent conductors

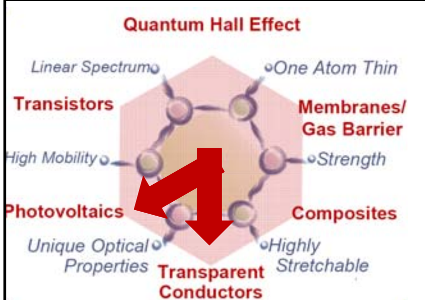

Requirements:
High transparency (T), low sheet resistance (Rs)
Dominant material: ITO (indium tin oxide)
(90% In_2O_3 10% SnO_2)T≈ 80% Rs =10-300Ω
ITOs limitations:

- Scarcity
- difficulties in patterning, processing requirements
- Sensitivity to acidic or basic environments
- Brittle
- Wear resistance

One atom thin,
High mobility:

Graphene: T = 97.7%, Rs=6kΩ

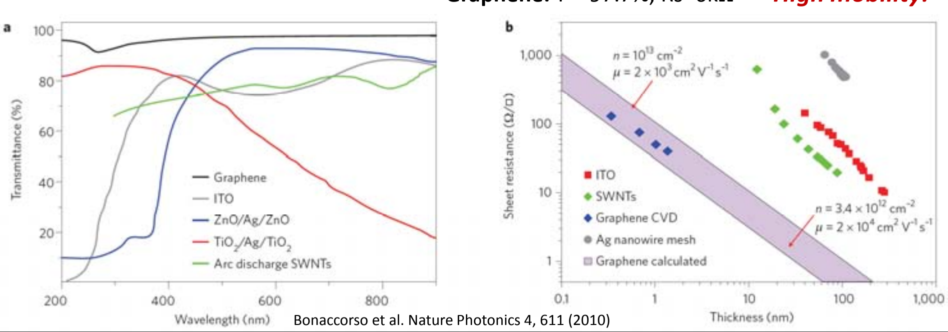

Bonaccorso et al. Nature Photonics 4, 611 (2010)

Transparent conductors

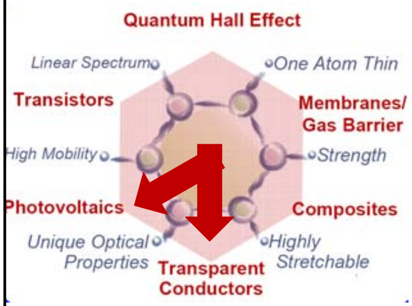

Requirements:
High transparency (T), low sheet resistance (Rs)
Graphene: T = 97.7%, Rs=6kΩ
doped **CVD** flakes could outperform ITO and others
LPE (Liquid phase exfolation): Rs higher, T=90%
but cheaper, easier to scale → application with cost reduction

Bonaccorso et al. Nature Photonics 4, 611 (2010)

Transparent conductors

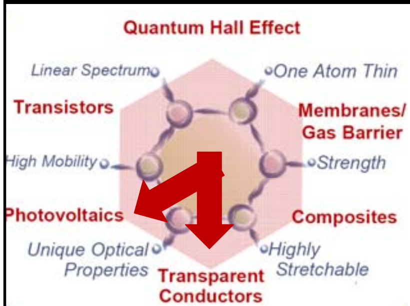

CVD growth GTCF (Graphene Transparent Film)

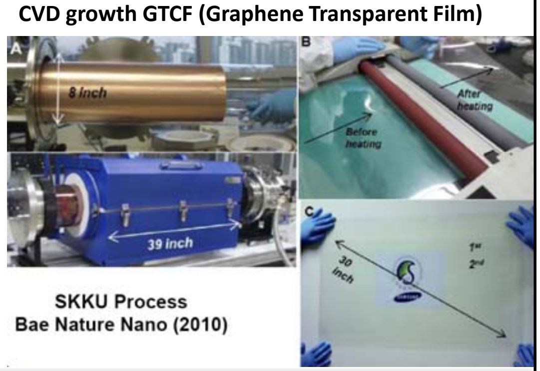

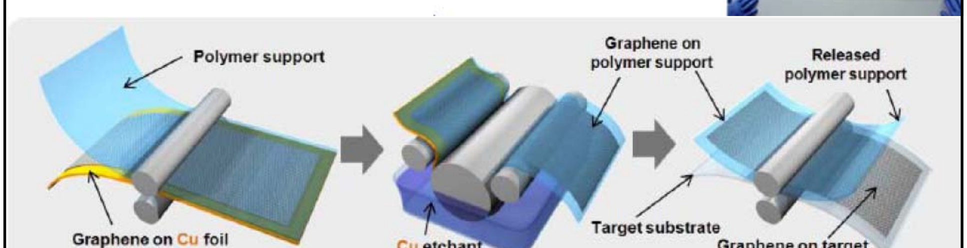

Bonaccorso et al. Nature Photonics 4, 611 (2010)

Applications of Transparent conductors

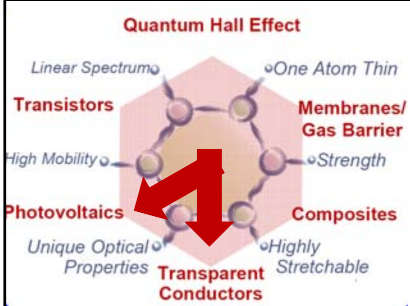

SKKU Touch screen

Bae, S. et al. Nature Nano (2010)

Touch screens

Resistive touch panel, by pressing the front conductive layer comes into contact with back one. Cost, brittleness, wear resistance, chemical durability main limitation of ITO . Graphene fullfills.

Capacitive touch screens (iPhone) Glass coated with ITO, human body as conductor changes the capacitance. → Reduce cost, improve performance.

Flexible Smart windows/bistabile displays

Depending on the orientation of the liquid crystal droplets milky film or transparent one.

Due to high cost of ITO not-widely used. G is even flexible. Also for zero power bistabile displays.

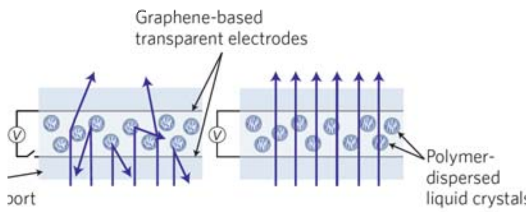

Bonaccorso et al. Nature Photonics 4, 611 (2010)

Applications of Transparent conductors

Transparent graphene film

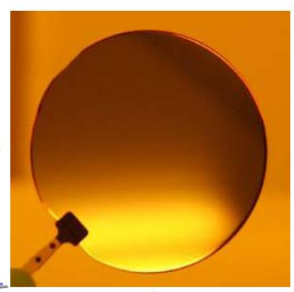

4 inch scale graphene film on Stretchable Substrate

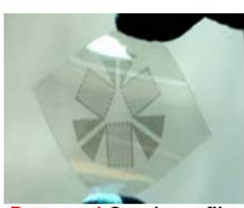

Patterned Graphene film on PET

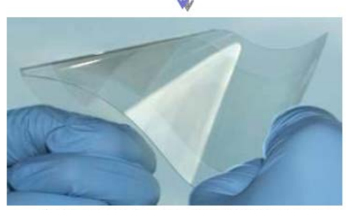

4 inch scale graphene film on Flexible Substrate

SUNG KYUN KWA UNIVERSITY

Bonaccorso et al. Nature Photonics 4, 611 (2010)

Applications of Transparent conductors

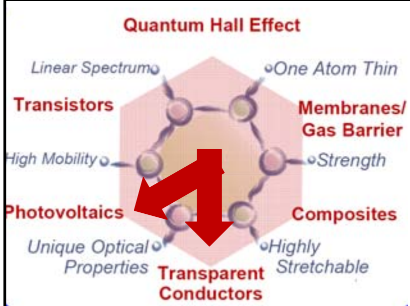

Flexible, Foldable AMOLED Display

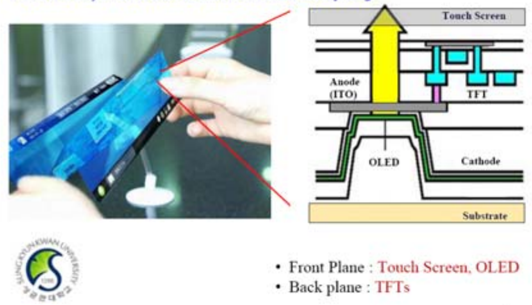

SKKU Touch screen

Bae, S. et al. Nature Nano (2010)

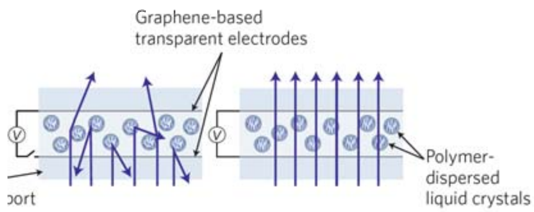

Bonaccorso et al. Nature Photonics 4, 611 (2010)

Photovoltaic cells

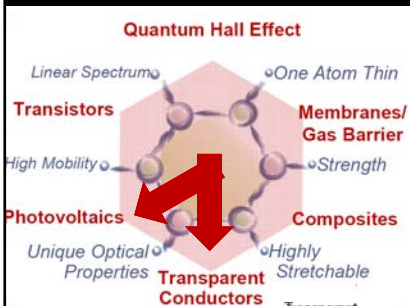

It converts light to electricity.
It consists photo active part (ph → e-h), electrodes
Currently silicon cells dominating η ≈ 25% ,
Organic cells are economical, η ≈ few%

Function of Graphene:

- Transparent conduction window
- Photoactive material (claim η >12% is possible)
- channel for charge transport

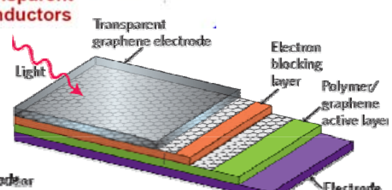

Dye-sensitized cell
with G as a TiO bridge η ≈ 7%
with G counter electrode η ≈ 4.5%
instead of Pt η ≈ 6.3% → cheaper

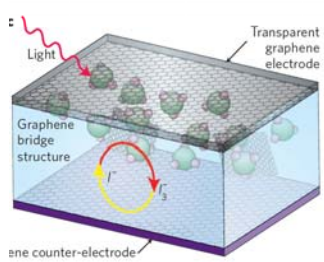

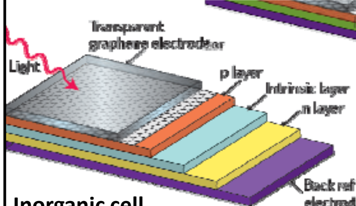

Organic cell
Polimer for light absorption and charge transfer

Inorganic cell

Bonaccorso et al. Nature Photonics 4, 611 (2010)

Saturable absorbers, ultrafast laser

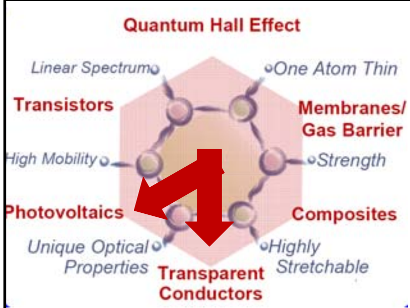

Laser sources with nano to subpicosec pulses
Important in physics, biology, chemistry and also applications: e.g. eye surgery, circuit board manufacturing, trimming electronic components.
Principle: Saturable absorber (SA) turns a continious wave output to ultrafast pulses
Requirements for SA:
Fast response, strong nonlinearity, broad wavelength, low optical loss, high power handling, low power consumption, low cost
Graphene: linear dispersion, ultrafast carrier dynamics, Pauli blocking → ultra broadband, fast SA

Basic principle

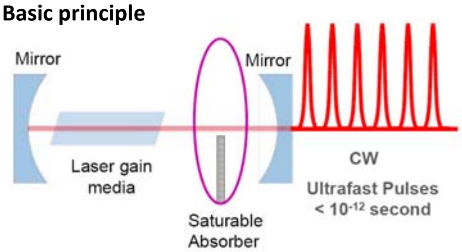

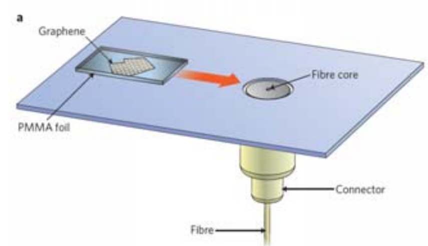

Bonaccorso et al. Nature Photonics 4, 611 (2010)

Teraherz devices

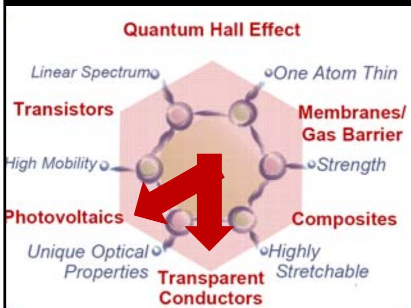

Radiation in 0.3 -10 THz range (30um to 1mm)
Important for biomedical imaging , spectroscopy.
Unexplored, lack of efficient sources and detectors.

Graphene plasma waves, bilayer graphene tunable band gap, gap of nanoribbons are in this range.

Teraherz emission in optically pumped graphene is demonstrated. → THz generation
G can be used for THz detection and frequency conversion.

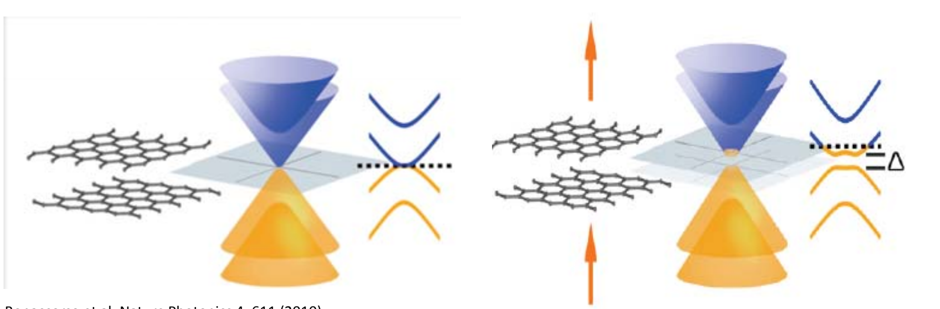

Bonaccorso et al. Nature Photonics 4, 611 (2010)

Transistors

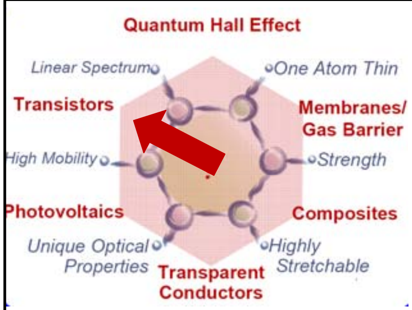

Zero band gap → small on-off ratio
For **Radio frequency** (RF) **transistors** e.g. amplifier, mixers, e.g. in wireless systems not a problem.
f_T : cut off frequency , Current gain goes to 1.
f_{max}: max freq. of oscillation with power gain 1
High mobility → high frequency
f_T = 300GHz exfoilated graphene
f_T = 155GHz with 40nm gate length in industry compatible graphene transistor.
CVD growth graphene deposited on diamond like carbon film instead of SiO_2 (to enhance mobility)

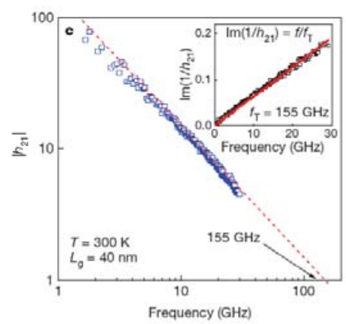

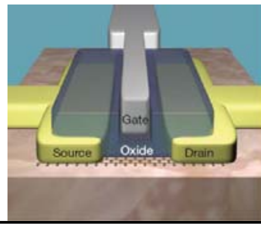

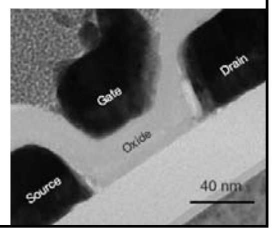

Wu Nature 472, 74 (2011)

Transistors

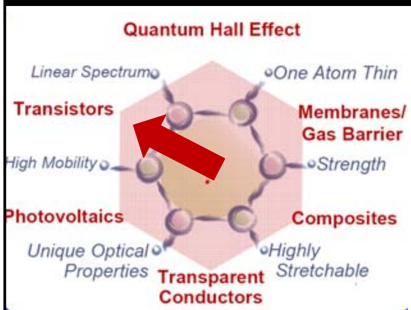

Zero band gap → small on-off ratio
For **Radio frequency** (RF) **transistors** e.g. amplifier, mixers, e.g. in wireless systems not a problem.
f_T : cut off frequency , Current gain goes to 1.
f_{max}: max freq. of oscillation with power gain 1

For high f_T graphene is compatitive.
With 20nm channel length intrinsic $f_T \approx$ few THz is expected. Possible to scale down.

f_{max} is quite low compare to Si and III-Vs.
Reason: weak saturation of drain current due to lack of band gap and high contact resistance.

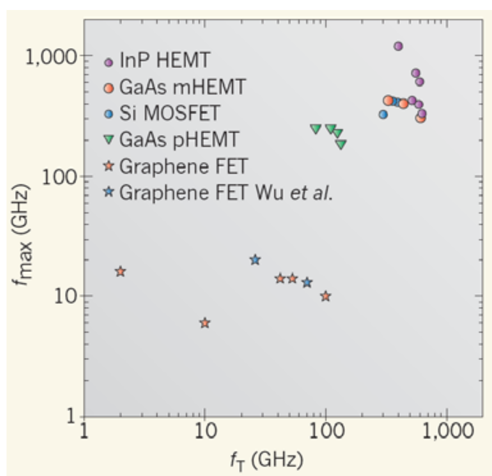

Schwierz Nature 472, 41 (2011)

Transistors

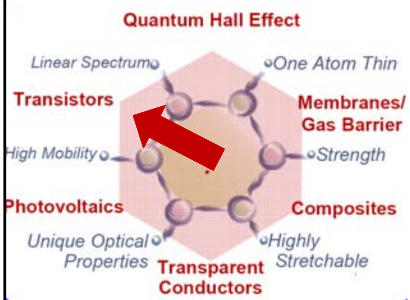

Zero band gap → small on-off ratio
For **Radio frequency** (RF) **transistors** e.g. amplifier, mixers, e.g. in wireless systems not a problem.
f_T : cut off frequency , Current gain goes to 1.
f_{max}: max freq. of oscillation with power gain 1

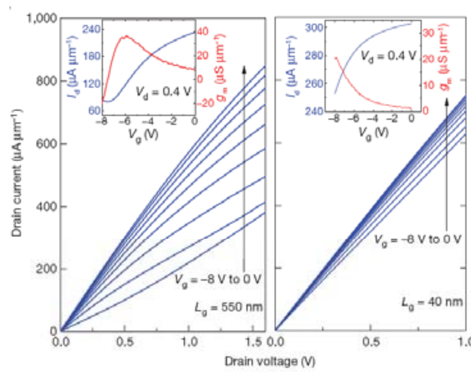

For high f_T graphene is compatitive.
With 20nm channel length intrinsic $f_T \approx$ few THz is expected. Possible to scale down.

f_{max} is quite low compare to Si and III-Vs.
Reason: weak saturation of drain current due to lack of band gap and high contact resistance.

Drawbacks:
- No saturation of I_D for large V_{SD}
- Small effect of V_g due to $R_{contact}$

Schwierz Nature 472, 41 (2011)

Transistors

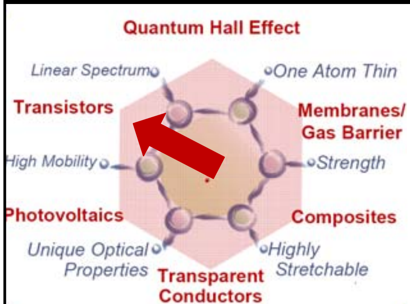

Zero band gap → small on-off ratio
For **Radio frequency** (RF) **transistors** e.g. amplifier, mixers, e.g. in wireless systems not a problem.
f_T : cut off frequency , Current gain goes to 1.
f_{max}: max freq. of oscillation with power gain 1

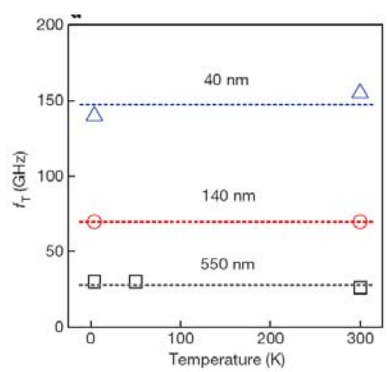

For high f_T graphene is compatitive.
With 20nm channel length intrinsic $f_T \approx$ few THz is expected. Possible to scale down.

f_{max} is quite low compare to Si and III-Vs.
Reason: weak saturation of drain current due to lack of band gap and high contact resistance.

Operates from 300K to 4K!

Wu Nature 472, 74 (2011)

Graphene + Hybrid systems

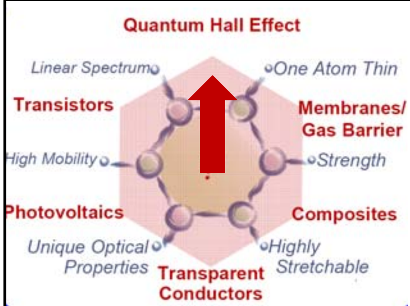

Advantages:

- 2DEG compatible with S and F contacts
- Simple production, flexible structuring
  Qdots, Y – junctions, loops
- Large mobility, long spin mean free path
  $\mu = 6\ 10^5\ cm^2/Vs$ @77K l_e~3µm, l_s ~2µm@RT
- 1 atom thin (→ Local probes)
- Exotic electron structure
  Dirac spectrum, isospin, pseudo spin

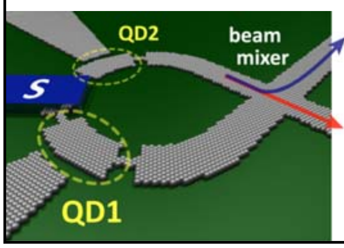

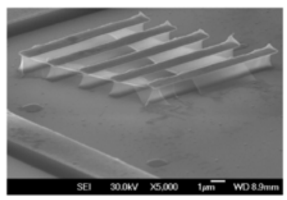

N. Tombros arXiv:1009.4213 (2010)

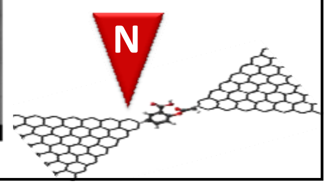

Carbon Nanostructures – Part II

I. Graphene

Outline:

- Introduction (Making graphene, Applications, etc.)
- Band structure
- Physics of Dirac electrons (Barry phase, Klein tunneling)
- Half-Integer Quantum Hall Effect
- Mobility in Graphene (ways to improve…)

References:

- E. McCann Graphene monolayers Lancaster University, UK Tight-binding model, QHE
- C. Beenakker, Reviews of Modern Physics, 80, 1337 (2008)
- L. Tapaszto & J. Cserti talks, MAFIHE Teli Iskola a Grafenrol 2011, ELTE
- A. Geim talk, TNT Conference 2010 http://www.tntconf.org/2010/Presentaciones/TNT2010_Geim.pdf
- N.Peres, F. Guinea and A.H. Castro Neto, PRB 73, 125411 (2006)

BANDSTRUCTURE OF GRAPHENE

Graphite

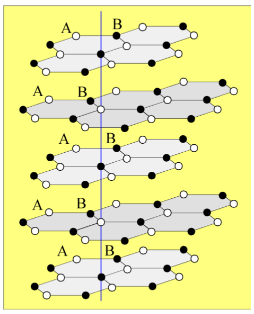

Three dimensional layered material with hexagonal 2D layers [shown here with Bernal (AB) stacking]

Monolayer

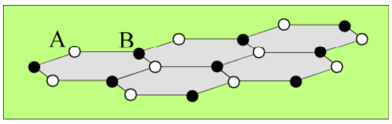

Two dimensional material; zero gap semiconductor; Dirac spectrum of electrons

Bilayer

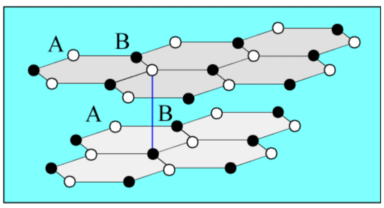

1 Tight binding model of monolayer graphene

1.1 sp^2 hybridisation

Carbon has 6 electrons: 2 are core electrons, 4 are valence electrons – one 2s and three 2p orbitals

sp^2 hybridisation
- single 2s and two 2p orbitals hybridise forming three "σ bonds" in the x-y plane

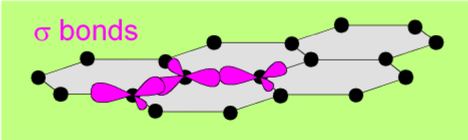

- remaining 2p$_z$ orbital ["π" orbital] exists perpendicular to the x-y plane

only π orbital relevant for energies of interest for transport measurements – so keep only this one orbital per site in the tight binding model

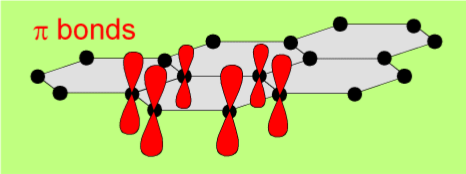

1 Tight binding model of monolayer graphene

1.2 lattice of graphene

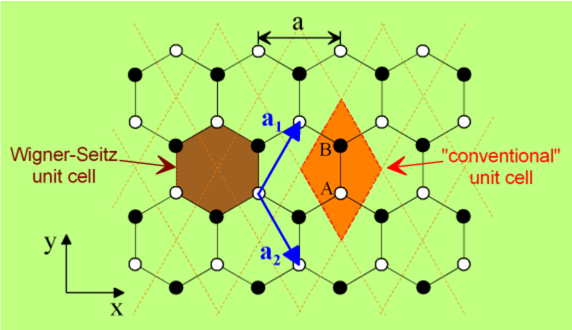

2 different atomic sites – 2 triangular sub-lattices

1 Tight binding model of monolayer graphene

1.3 reciprocal lattice

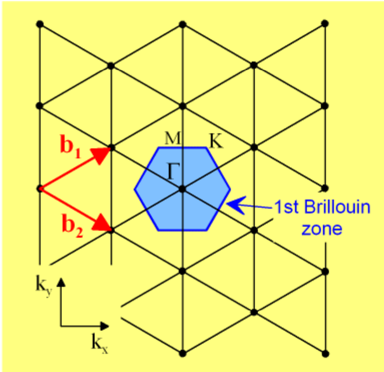

triangular reciprocal lattice

– hexagonal Brillouin zone

1 Tight binding model of monolayer graphene

1.4 Bloch functions

We take into account one π orbital per site, so there are two orbitals per unit cell.

Bloch functions

$$\Phi_A(\vec{k},\vec{r}) = \frac{1}{\sqrt{N}} \sum_{\vec{R}_A}^{N} e^{i\vec{k}.\vec{R}_A} \varphi_A(\vec{r}-\vec{R}_A)$$

$$\Phi_B(\vec{k},\vec{r}) = \frac{1}{\sqrt{N}} \sum_{\vec{R}_B}^{N} e^{i\vec{k}.\vec{R}_B} \varphi_B(\vec{r}-\vec{R}_B)$$

sum over all type B atomic sites in N unit cells

atomic wavefunction

1 Tight binding model of monolayer graphene

1.4 Bloch functions

We take into account one π orbital per site, so there are two orbitals per unit cell.

Bloch functions : label with j = 1 [A sites] or 2 [B sites]

$$\Phi_j(\vec{k},\vec{r}) = \frac{1}{\sqrt{N}}\sum_{\vec{R}_j}^{N} e^{i\vec{k}.\vec{R}_j}\varphi_j(\vec{r}-\vec{R}_j)$$

sum over all type j atomic sites in N unit cells

atomic wavefunction

1 Tight binding model of monolayer graphene

1.5 Secular equation

Eigenfunction Ψ_j (for j = 1 or 2) is written as a linear combination of Bloch functions:

$$\Psi_j(\vec{k},\vec{r}) = \sum_{j'=1}^{2} C_{jj'}(\vec{k})\Phi_{j'}(\vec{k},\vec{r})$$

Eigenvalue E_j (for j = 1 or 2) is written as :

$$E_j(\vec{k}) = \frac{\langle \Psi_j | H | \Psi_j \rangle}{\langle \Psi_j | \Psi_j \rangle}$$

substitute expression in terms of Bloch functions

$$E_j(\vec{k}) = \frac{\sum_{i,l}^{2} C_{ji}^{*} C_{jl} \langle \Phi_i | H | \Phi_l \rangle}{\sum_{i,l}^{2} C_{ji}^{*} C_{jl} \langle \Phi_i | \Phi_l \rangle} \equiv \frac{\sum_{i,l}^{2} H_{il} C_{ji}^{*} C_{jl}}{\sum_{i,l}^{2} S_{il} C_{ji}^{*} C_{jl}}$$

defining transfer integral matrix elements $H_{il} = \langle \Phi_i | H | \Phi_l \rangle;$ and overlap integral matrix elements $S_{il} = \langle \Phi_i | \Phi_l \rangle$

1 Tight binding model of monolayer graphene

1.5 Secular equation

$$E_j(\vec{k}) = \frac{\sum_{i,l}^{2} H_{il} C_{ji}^{*} C_{jl}}{\sum_{i,l}^{2} S_{il} C_{ji}^{*} C_{jl}}$$

If the H_{il} and S_{il} are known, we can find the energy by minimising with respect to C^{*}_{jm}:

$$\frac{\partial E_j}{\partial C_{jm}^{*}} = \frac{\sum_{l}^{2} H_{ml} C_{jl}}{\sum_{i,l}^{2} S_{il} C_{ji}^{*} C_{jl}} - \frac{\sum_{i,l}^{2} H_{il} C_{ji}^{*} C_{jl} \sum_{l}^{2} S_{ml} C_{jl}}{\left(\sum_{i,l}^{2} S_{il} C_{ji}^{*} C_{jl}\right)^{2}}$$

$$\frac{\partial E_j}{\partial C_{jm}^{*}} = 0 \quad \Rightarrow \quad \sum_{l=1}^{2} H_{ml} C_{jl} = E_j \sum_{l=1}^{2} S_{ml} C_{jl}$$

1 Tight binding model of monolayer graphene

1.5 Secular equation

$$\sum_{l=1}^{2} H_{ml} C_{jl} = E_j \sum_{l=1}^{2} S_{ml} C_{jl}$$

Explicitly write out sums:

$$m = 1 \quad \Rightarrow \quad H_{11} C_{j1} + H_{12} C_{j2} = E_j \left(S_{11} C_{j1} + S_{12} C_{j2} \right)$$

$$m = 2 \quad \Rightarrow \quad H_{21} C_{j1} + H_{22} C_{j2} = E_j \left(S_{21} C_{j1} + S_{22} C_{j2} \right)$$

Write as a matrix equation:

$$\begin{pmatrix} H_{11} & H_{12} \\ H_{21} & H_{22} \end{pmatrix} \begin{pmatrix} C_{j1} \\ C_{j2} \end{pmatrix} = E_j \begin{pmatrix} S_{11} & S_{12} \\ S_{21} & S_{22} \end{pmatrix} \begin{pmatrix} C_{j1} \\ C_{j2} \end{pmatrix}$$

$$HC_j = E_j S C_j$$

Secular equation gives the eigenvalues:

$$\det(H - ES) = 0$$

1 Tight binding model of monolayer graphene
1.6 Calculation of transfer and overlap integrals

$$H_{ij} = \langle \Phi_i | H | \Phi_j \rangle; \qquad S_{ij} = \langle \Phi_i | \Phi_j \rangle \qquad \Phi_j(\vec{k},\vec{r}) = \frac{1}{\sqrt{N}} \sum_{\vec{R}_j}^{N} e^{i\vec{k}.\vec{R}_j} \varphi_j(\vec{r}-\vec{R}_j)$$

Diagonal matrix element

$$H_{AA} = \langle \Phi_A | H | \Phi_A \rangle = \frac{1}{N} \sum_{\vec{R}_{Ai}}^{N} \sum_{\vec{R}_{Aj}}^{N} e^{i\vec{k}.(\vec{R}_{Aj}-\vec{R}_{Ai})} \langle \varphi_A(\vec{r}-\vec{R}_{Ai}) | H | \varphi_A(\vec{r}-\vec{R}_{Aj}) \rangle$$

Same site only:

$$H_{AA} = \frac{1}{N} \sum_{\vec{R}_{Ai}}^{N} \langle \varphi_A(\vec{r}-\vec{R}_{Ai}) | H | \varphi_A(\vec{r}-\vec{R}_{Ai}) \rangle = \langle \varphi_A(\vec{r}-\vec{R}_{Ai}) | H | \varphi_A(\vec{r}-\vec{R}_{Ai}) \rangle \equiv \varepsilon_0$$

$$S_{AA} = \frac{1}{N} \sum_{\vec{R}_{Ai}}^{N} \langle \varphi_A(\vec{r}-\vec{R}_{Ai}) | \varphi_A(\vec{r}-\vec{R}_{Ai}) \rangle = \langle \varphi_A(\vec{r}-\vec{R}_{Ai}) | \varphi_A(\vec{r}-\vec{R}_{Ai}) \rangle \equiv 1$$

A and B sites are chemically identical:

$$H_{AA} = H_{BB} = \varepsilon_0 \qquad S_{AA} = S_{BB} = 1$$

1 Tight binding model of monolayer graphene
1.6 Calculation of transfer and overlap integrals

Off-diagonal matrix element

$$H_{AB} = \langle \Phi_A | H | \Phi_B \rangle = \frac{1}{N} \sum_{\vec{R}_{Ai}}^{N} \sum_{\vec{R}_{Bj}}^{N} e^{i\vec{k}.(\vec{R}_{Bj}-\vec{R}_{Ai})} \langle \varphi_A(\vec{r}-\vec{R}_{Ai}) | H | \varphi_B(\vec{r}-\vec{R}_{Bj}) \rangle$$

Every A site has 3 B nearest neighbours:

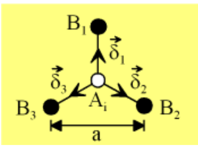

$$\vec{\delta}_1 = R_{B1} - R_{Ai} = \left(0, \frac{a}{\sqrt{3}}\right); \quad \vec{\delta}_2 = R_{B2} - R_{Ai} = \left(\frac{a}{2}, -\frac{a}{2\sqrt{3}}\right);$$

$$\vec{\delta}_3 = R_{B3} - R_{Ai} = \left(-\frac{a}{2}, -\frac{a}{2\sqrt{3}}\right)$$

$$H_{AB} = \frac{1}{N} \sum_{\vec{R}_{Ai}}^{N} \left[\sum_{\vec{\delta}_j=1}^{3} e^{i\vec{k}.\vec{\delta}_j} \langle \varphi_A(\vec{r}-\vec{R}_{Ai}) | H | \varphi_B(\vec{r}-\vec{R}_{Bj}) \rangle \right] = \sum_{\vec{\delta}_j=1}^{3} e^{i\vec{k}.\vec{\delta}_j} \langle \varphi_A(\vec{r}-\vec{R}_{Ai}) | H | \varphi_B(\vec{r}-\vec{R}_{Bj}) \rangle$$

Parameterise nearest neighbour transfer integral:

$$\gamma_0 = -\langle \varphi_A(\vec{r}-\vec{R}_{Ai}) | H | \varphi_B(\vec{r}-\vec{R}_{Bj}) \rangle \qquad s = \langle \varphi_A(\vec{r}-\vec{R}_{Ai}) | \varphi_B(\vec{r}-\vec{R}_{Bj}) \rangle$$

$$\Rightarrow \quad H_{AB} = -\gamma_0 f(\vec{k}); \qquad f(\vec{k}) = \sum_{\vec{\delta}_j=1}^{3} e^{i\vec{k}.\vec{\delta}_j} \qquad \Rightarrow \quad S_{AB} = s\, f(\vec{k})$$

1 Tight binding model of monolayer graphene
1.6 Calculation of transfer and overlap integrals

Off-diagonal matrix element

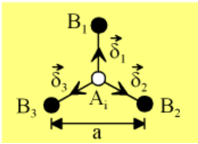

$$\vec{\delta}_1 = R_{B1} - R_{Ai} = \left(0, \frac{a}{\sqrt{3}}\right); \quad \vec{\delta}_2 = R_{B2} - R_{Ai} = \left(\frac{a}{2}, -\frac{a}{2\sqrt{3}}\right);$$

$$\vec{\delta}_3 = R_{B3} - R_{Ai} = \left(-\frac{a}{2}, -\frac{a}{2\sqrt{3}}\right)$$

$$f\left(\vec{k}\right) = \sum_{\vec{\delta}_j=1}^{3} e^{i\vec{k}.\vec{\delta}_j} = e^{ik_y a/\sqrt{3}} + 2e^{-ik_y a/2\sqrt{3}} \cos\left(\frac{k_x a}{2}\right)$$

1 Tight binding model of monolayer graphene
1.7 Calculation of energy

$$H = \begin{pmatrix} \varepsilon_0 & -\gamma_0 f\left(\vec{k}\right) \\ -\gamma_0 f^*\left(\vec{k}\right) & \varepsilon_0 \end{pmatrix}; \quad S = \begin{pmatrix} 1 & sf\left(\vec{k}\right) \\ sf^*\left(\vec{k}\right) & 1 \end{pmatrix}$$

Secular equation gives the eigenvalues:

$$\det(H - ES) = 0$$

$$\det\begin{pmatrix} \varepsilon_0 - E & -(\gamma_0 + Es) f\left(\vec{k}\right) \\ -(\gamma_0 + Es) f^*\left(\vec{k}\right) & \varepsilon_0 - E \end{pmatrix} = 0$$

$$(E - \varepsilon_0)^2 - (\gamma_0 + Es)^2 \left|f\left(\vec{k}\right)\right|^2 = 0$$

$$E = \frac{\varepsilon_0 \pm \gamma_0 \left|f\left(\vec{k}\right)\right|}{1 \mp s\left|f\left(\vec{k}\right)\right|}$$

1 Tight binding model of monolayer graphene

1.7 Calculation of energy

$$E = \frac{\varepsilon_0 \pm \gamma_0 \left| f(\vec{k}) \right|}{1 \mp s \left| f(\vec{k}) \right|}$$

Typical parameter values [quoted in Saito *et al*]:

$$\varepsilon_0 = 0 \,,\ \gamma_0 = 3.033eV \,,\ s = 0.129$$

$$f(\vec{k}) = e^{ik_y a/\sqrt{3}} + 2e^{-ik_y a/2\sqrt{3}} \cos\left(\tfrac{k_x a}{2}\right)$$

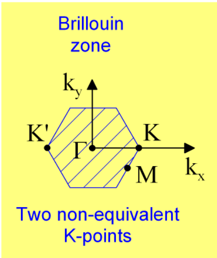

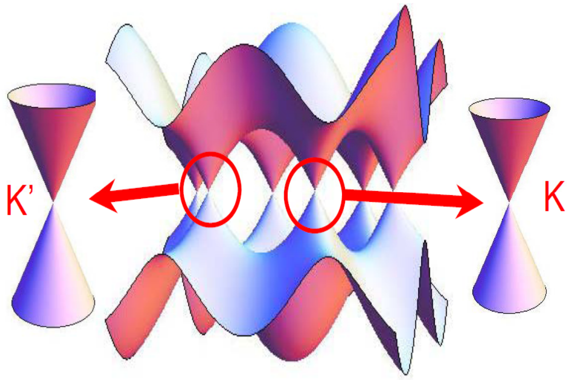

→ Gapless semiconductor

2 Expansion near the K points

2.1 Exactly at the K point

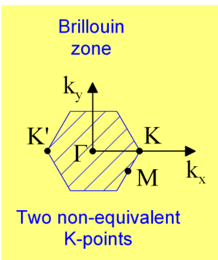

$$\vec{K} = \left(\frac{4\pi}{3a}, 0\right)$$

$$\vec{\delta}_1 = \left(0, \frac{a}{\sqrt{3}}\right); \quad \Rightarrow \quad K.\vec{\delta}_1 = 0$$

$$\vec{\delta}_2 = \left(\frac{a}{2}, -\frac{a}{2\sqrt{3}}\right); \quad \Rightarrow \quad K.\vec{\delta}_2 = \frac{2\pi}{3}$$

$$\vec{\delta}_3 = \left(-\frac{a}{2}, -\frac{a}{2\sqrt{3}}\right); \quad \Rightarrow \quad K.\vec{\delta}_3 = -\frac{2\pi}{3}$$

$$f(\vec{K}) = \sum_{\vec{\delta}_j = 1}^{3} e^{i\vec{K}.\vec{\delta}_j} = e^{0} + e^{2\pi i/3} + e^{-2\pi i/3} = 0$$

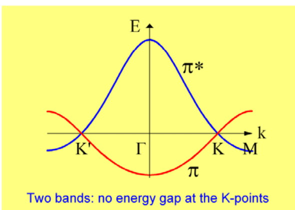

At the corners of the Brillouin zone (K points), electron states on the A and B sub-lattices decouple and have exactly the same energy

K points also referred to as "valleys"

2 Expansion near the K points

2.1 Exactly at the K point

6 corners of the Brillouin zone (K points), but only two are non-equivalent

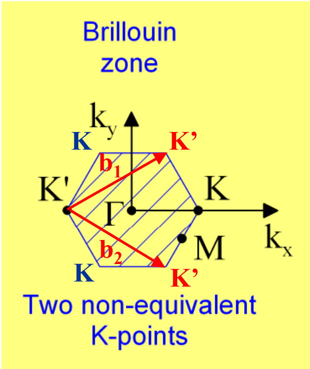

We consider two K points with the following wave vectors:

$$\vec{K}=\left(\frac{4\pi}{3a},0\right);\quad \vec{K}'=\left(-\frac{4\pi}{3a},0\right)$$

2 Expansion near the K points

2.2 Linear expansion

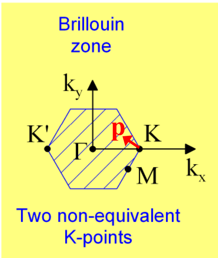

Consider two non-equivalent K points:

$$\vec{K},\vec{K}'=\xi\left(\frac{4\pi}{3a},0\right);\qquad \xi=\pm 1$$

and small momentum near them:

$$\vec{k}=\xi\left(\frac{4\pi}{3a},0\right)+\frac{\vec{p}}{\hbar}$$

2 Expansion near the K points

2.2 Linear expansion

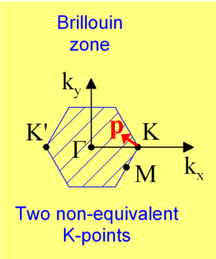

Consider two non-equivalent K points:

$$\vec{K},\vec{K}'=\xi\left(\frac{4\pi}{3a},0\right);\qquad \xi=\pm1$$

and small momentum near them:

$$\vec{k}=\xi\left(\frac{4\pi}{3a},0\right)+\frac{\vec{p}}{\hbar}$$

Linear expansion in small momentum: $f(\vec{k})=-\frac{\sqrt{3}a}{2\hbar}(\xi p_x-ip_y)+O(pa/\hbar)^2$

$$H=\begin{pmatrix}0 & -\gamma_0 f(\vec{k})\\ -\gamma_0 f^*(\vec{k}) & 0\end{pmatrix}\approx v\begin{pmatrix}0 & \xi p_x-ip_y\\ \xi p_x+ip_y & 0\end{pmatrix}$$

$$S=\begin{pmatrix}1 & sf(\vec{k})\\ sf^*(\vec{k}) & 1\end{pmatrix}\approx\begin{pmatrix}1 & 0\\ 0 & 1\end{pmatrix}+O\left(\frac{spa}{\hbar}\right)\qquad v=\frac{\sqrt{3}a\gamma_0}{2\hbar}\approx10^6\,m/s$$

2 Expansion near the K points

2.2 Linear expansion

$$H=\begin{pmatrix}0 & -\gamma_0 f(\vec{k})\\ -\gamma_0 f^*(\vec{k}) & 0\end{pmatrix}\approx v\begin{pmatrix}0 & \xi p_x-ip_y\\ \xi p_x+ip_y & 0\end{pmatrix}$$

$$S=\begin{pmatrix}1 & sf(\vec{k})\\ sf^*(\vec{k}) & 1\end{pmatrix}\approx\begin{pmatrix}1 & 0\\ 0 & 1\end{pmatrix}+O\left(\frac{spa}{\hbar}\right)\qquad v=\frac{\sqrt{3}a\gamma_0}{2\hbar}\approx10^6\,m/s$$

New notation for components on A and B sites

$$C_j=\begin{pmatrix}C_{j1}\\ C_{j2}\end{pmatrix}\Leftrightarrow\psi=\begin{pmatrix}\psi_A\\ \psi_B\end{pmatrix}$$

$$S^{-1}HC_j=E_jC_j\quad\Rightarrow\quad v\begin{pmatrix}0 & \xi p_x-ip_y\\ \xi p_x+ip_y & 0\end{pmatrix}\begin{pmatrix}\psi_A\\ \psi_B\end{pmatrix}=E\begin{pmatrix}\psi_A\\ \psi_B\end{pmatrix}$$

2 Expansion near the K points

2.3 Dirac-like equation

For one K point (e.g. ξ=+1) we have a 2 component wave function,

$$\psi = \begin{pmatrix} \psi_A \\ \psi_B \end{pmatrix}$$

with the following effective Hamiltonian:

$$H = v\begin{pmatrix} 0 & p_x - ip_y \\ p_x + ip_y & 0 \end{pmatrix} = v\begin{pmatrix} 0 & \pi^+ \\ \pi & 0 \end{pmatrix} = v\left(\sigma_x p_x + \sigma_y p_y\right) = v\vec{\sigma}.\vec{p}$$

$\pi = p_x + ip_y = pe^{i\varphi}$

$\pi^+ = p_x - ip_y = pe^{-i\varphi}$

Bloch function amplitudes on the AB sites ('pseudospin') mimic spin components of a relativistic Dirac fermion.

Pseudospin is an index that indicates on which of the two sublattices a quasi-particle is located

2 Expansion near the K points

2.3 Dirac-like equation

To take into account both K points (ξ=+1 and ξ=-1) we can use a 4 component wave function,

$$\psi = \begin{pmatrix} \psi_{AK} \\ \psi_{BK} \\ \psi_{AK'} \\ \psi_{BK'} \end{pmatrix}$$

with the following effective Hamiltonian:

$$H = v\begin{pmatrix} 0 & p_x - ip_y & 0 & 0 \\ p_x + ip_y & 0 & 0 & 0 \\ 0 & 0 & 0 & -p_x - ip_y \\ 0 & 0 & -p_x + ip_y & 0 \end{pmatrix}$$

Isospin K and K' valleys are also called isospin.

2 Expansion near the K points

2.3 Dirac-like equation

$$H = v\begin{pmatrix} 0 & \pi^{+} \\ \pi & 0 \end{pmatrix} = v\vec{\sigma}\cdot\vec{p} = vp\ \vec{\sigma}\cdot\vec{n}$$

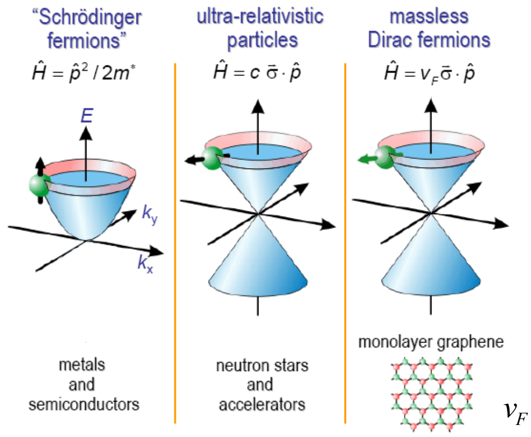

$v_F = c/300 = 10^6\ m/s$

Chiral electrons

pseudospin direction is linked to an axis determined by electronic momentum.

for conduction band electrons,

$$\vec{\sigma}\cdot\vec{n} = 1$$

valence band ('holes')

$$\vec{\sigma}\cdot\vec{n} = -1$$

It is due to symmetry of the honeycomb lattice

Basic transport characteristics

Measurement:

Graphene (blue) is etched to a Hall bar shape and contacted by metal leads (yellow). Si layer is doped, used as a backgate (G) . By applying voltage on G the chemical potential of graphene can be varied.

Effect of gate voltage, V_g?

$N = C_g V_g/e \quad \rightarrow \quad n \sim V_g \quad \rightarrow \quad k_F \sim \sqrt{V_g}$

Drude model:

$v_d \equiv \mu E,\ j \equiv env_d = en\mu E = \sigma E,\ \sigma = en\mu$

$\sigma = 1/\rho = \frac{e^2 n\tau}{m},\quad \mu = \frac{e\tau}{m},\quad R_H = \frac{V_y}{I} = \frac{E_y}{j_x} = -\frac{B}{ne}$

Measurement of Hall resistance allows to determine n.

Combining it with ρ, μ can be derived.

Fig. a: longitudinal resistance vs. Vg, ΔR≈ 100 times!

Fig. b: mobility and charge carrier density vs. Vg

- At V_g=0, R_H (and n) changes sign → boarder between e and h bands
- If V_g →0 R↗, however R is finite (≈4kOhm) at Dirac point although n=0. (No real OFF state.)
- mobility largest at Dirac point (V_g = 0).

$E(\vec{k}) = \hbar v_F|\vec{k}|$

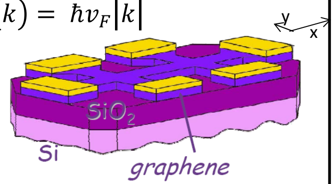

***R* vs. V_g characteristics**

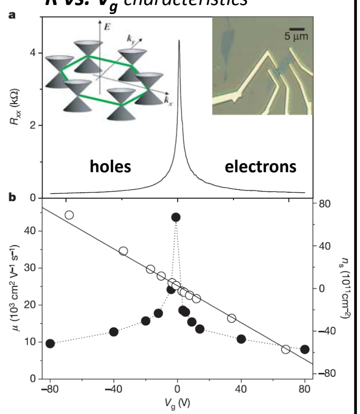

Nature **438**, 201 (2005)

3 Consequences of Dirac like spectrum 3.1 Berry's phase π

Massless Dirac fermions with Berry's phase π

$$H = v\begin{pmatrix} 0 & \pi^+ \\ \pi & 0 \end{pmatrix} = vp\begin{pmatrix} 0 & e^{-i\varphi} \\ e^{i\varphi} & 0 \end{pmatrix};$$

Solution: $E = vp \Leftrightarrow \psi(\varphi) = \frac{1}{\sqrt{2}}\begin{pmatrix} e^{-i\varphi/2} \\ e^{i\varphi/2} \end{pmatrix}$

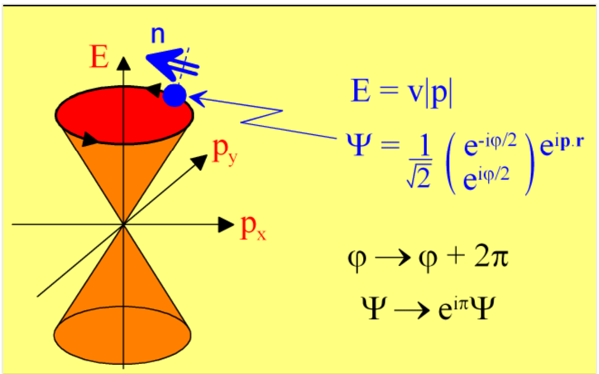

Making a loop around k=0 induces a phase shift of π.
Similar to the 360° rotation of an 1/2 e spin.

3.2 *Massless* Dirac Fermions?

Consider Quasi Classical Dynamics of Dirac electrons

$$\vec{v} \equiv \frac{1}{\hbar}\frac{\partial E}{\partial \vec{k}} = \frac{1}{\hbar}\hbar v_F \frac{\vec{k}}{|k|} = v_F \vec{e_k} = v_F^2 \frac{\vec{k}}{E},$$

thus $|v| = v_F$, $\vec{v}||\vec{k}$

→Speed of e is constant independent of momentum, like photons (v_F↔c)

What is m, effective mass?

$$\frac{1}{m} = \frac{1}{m_{xx}} = \frac{1}{\hbar^2}\frac{\partial^2 E}{\partial k_x^2}$$

For quadratic dispersion: $E = \frac{\hbar^2 k^2}{2m_{eff}}$, $m = m_{eff}$

For Dirac electrons, where $E(\vec{k}) = \hbar v_F|\vec{k}|$?

Naively 1/m= 0, but NOT. To calculate 1/m:

$$\frac{\partial^2 |k|}{\partial k_x^2} = \cdots = \frac{k_y^2}{|k|^3} \rightarrow \frac{1}{m_{xx}} = \frac{1}{\hbar} v_F \frac{k_y^2}{k^3}$$

$\frac{\partial |k|}{\partial k_x} = \frac{1}{2}\frac{2k_x}{|k|}$ → Effective mass depends on k

$$E(\vec{k}) = \pm\hbar v_F|\vec{k}|$$

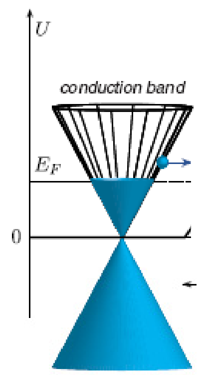

Beenakker, Reviews of Modern Physics, 80, 1337 (2008)

3.3 Klein tunneling and backscattering

$$\frac{1}{m_{xx}} = \frac{v_F}{\hbar}\frac{k_y^2}{|k|^3}$$

N-P junction:
Potential profile with a step of U_0 at a distance d

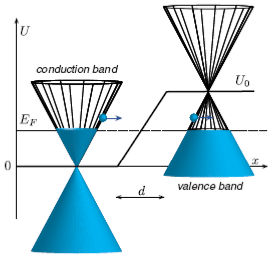

Klein scattering:
perfect transmission at normal incident

Evolution of group velocity:

$$\frac{dv_x}{dt} \equiv \frac{1}{m_{xx}}F_x = \frac{1}{m_{xx}}(-e)E_0 \quad (*)$$

In linear electrostatic potential (e.g. slope in Figure) :

$$V = E_0 x, \quad E_x = E_0, \quad F_x = -eE_0$$

At normal incident: $k_y = 0 \rightarrow \frac{dv_x}{dt} = 0 \rightarrow$ backscattering is avoided. Electron can propagate through an infinite high potential barrier.

$$\hbar\dot{\vec{k}} \equiv \vec{F} = -eE_0\overrightarrow{e_x} \quad (**)$$

Effect of the potential profile, U (see figure):

- k decreases and changes sign (**)
- based on (*), $\vec{v}$ stays constant, i.e. $\vec{v} = v_F\overrightarrow{e_x}$.

→ e ends up in the valence band

3.3 Klein tunneling and backscattering

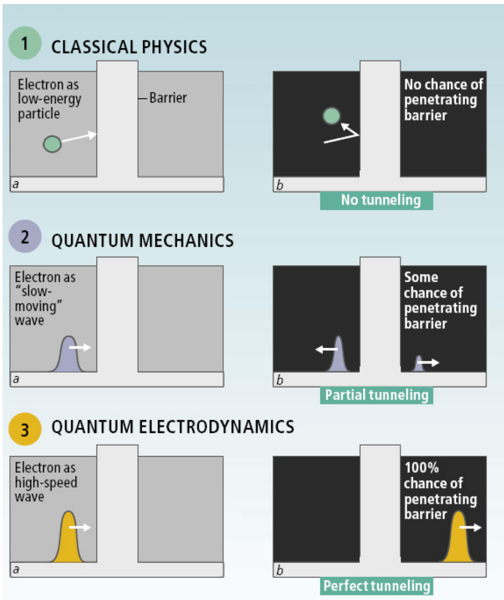

Beenakker, Reviews of Modern Physics, 80, 1337 (2008)

Geim, Kim, Sci.Am. 298, 90 (2008)

Klein tunneling and backscattering

Result of proper calculation
Wave function matching

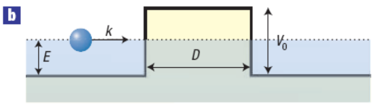

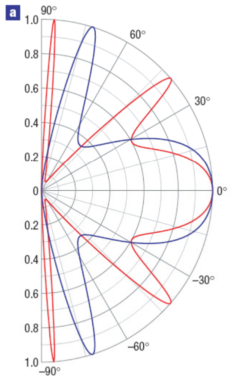

Transmission probability T through a 100-nm-wide barrier as a function of the incident angle, two different barrier height

Transmission probability vs. D of normally incident electrons
- in single- and bi-layer graphene (red and blue curves,respectively) and in a non-chiral zero-gap semiconductor (green curve)

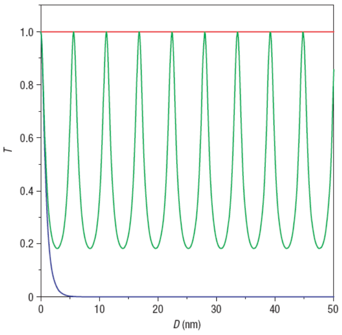

→ Difficult to measure whether it is 100%, since e-s out of normal incident also arrive

Katsnelson et al Nature Physics, 2, 620 (2006)

Klein backscattering & Fabry-Perot Interferences

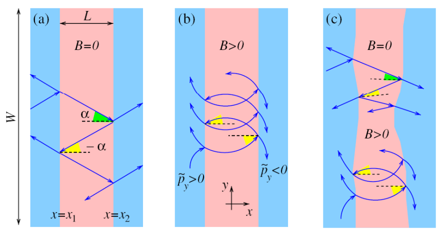

Interferences on P-N-P junction
When incident angle, α is varied from positive to negative, phase of the reflection amplitude (R) jumps π. Its sign changes. (At α=0, R=0).

If α<>0 → R>0, several scatterings in P-N- P → interference pattern
Accumulated phase in one circle:

$$\Delta\theta = 2\theta_{WBK} + \Delta\theta_1 + \Delta\theta_2$$

where θ_{WBK} phase from travelling in N
$\Delta\theta_1, \Delta\theta_2$ Klein back reflection phase of the interfaces

At B=0 (see Fig. a) the incident angles $\Delta\theta_{1(2)}$ at P-N and N-P have opposite signs → jumps in $\Delta\theta_1$, $\Delta\theta_2$ cancels

At B>0 (see Fig. b), trajectories are curved, → incident angles at P-N and N-P can be equal
In this case one can show that $\Delta\theta_1+\Delta\theta_2 = \pi$ (It is the Barry phase previously derived!)
Thus for B=0 ↗ and trajectories with small p_y π shift is expected (i.e. sign change) transmission amplitude

(Fig.c) one can show, it is robust against barrier roughness

Shytov et al. PRL 101, 156804 (2008)

Klein backscattering & Fabry-Perot Interferences

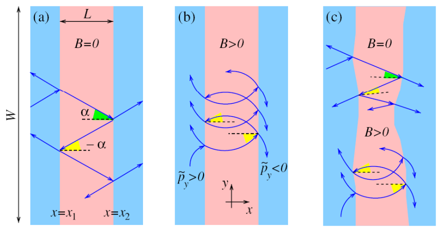

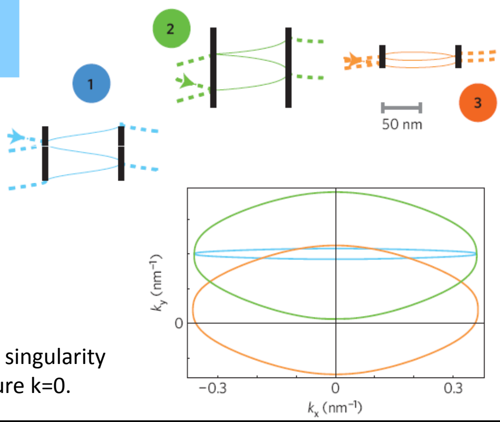

Remark (Barry-phase):

Trajectory in Fig.a corresponds to **1**
Trajectory in Fig.b corresponds to **3**
The main difference that during one circle between P-N and N-P:
the k vactor of **3** goes around k=0
while for **1** NOT.
This generates the Barry phase:
Due to the chiral symmetry, topological singularity at degenerecy point of the band structure k=0.

Shytov et al. PRL 101, 156804 (2008)

Klein backscattering & Fabry-Perot Interferences

N-P-N device

Separate gating by backgate and topgate
Topgate width=20nm! → ballistic

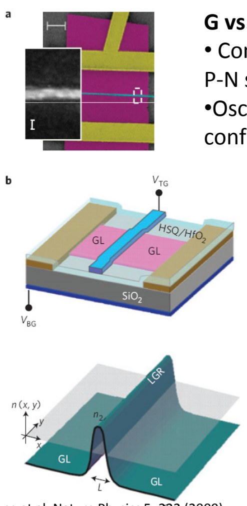

G vs. V_{TG} vs. V_{BG}

- Conductance is lower when N-P-N setting instead of N-N-N
- Oscillations at N-P-N configuration:
  - V_{TG} varies pot. barrier → $\delta\theta_{WBK}$ → oscillations
  - Oscillatory G is induced by trajectories with incident angle where neither T, nor R is large (i.e. α not too small)

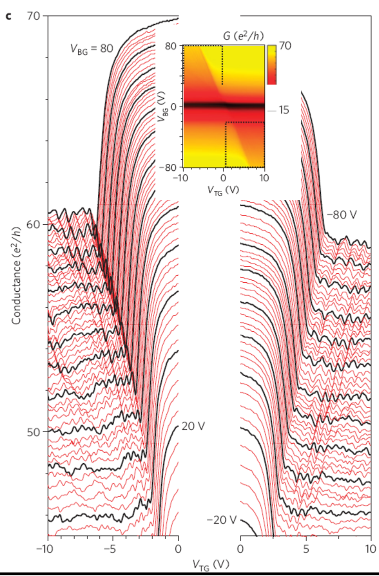

Young et al. Nature Physics 5, 222 (2009)

Klein backscattering & Fabry-Perot Interferences

N-P-N device

Separate gating by backgate and topgate
Topgate width=20nm! → ballistic

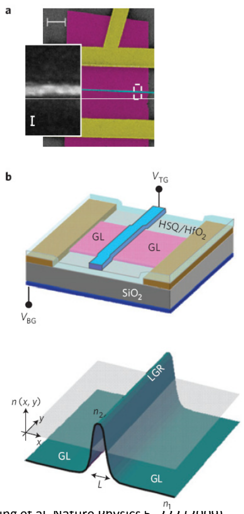

Young et al. Nature Physics 5, 222 (2009)

G oscillations vs. B *(Dots experiment, line theory)*

At different B fields (B=0, 200, 400, 600, 800mT from bottom to top) the oscillations of G.

In this B range ≈ π shift is induced in the interference pattern.

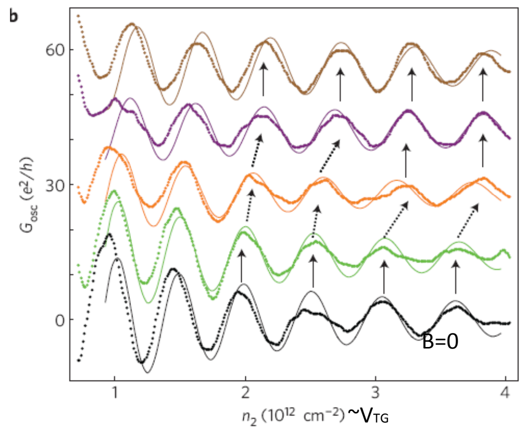

Half Integer Quantum Hall effect in graphene

Novoselov *et al*, Nature 438, 197 (2005)

Graphene in Hall geometry

Sample width of 200nm

- Sample: Hall geometry is etched from graphene flakes by oxigen plasma (a)

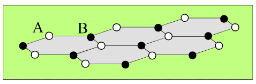

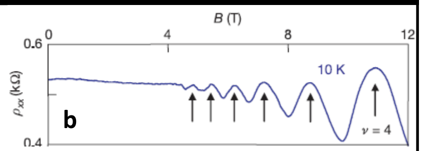

Longitudinal and Hall measurements vs B field

Conventional way of QHE measurement

QHE vs. density (gate voltage)

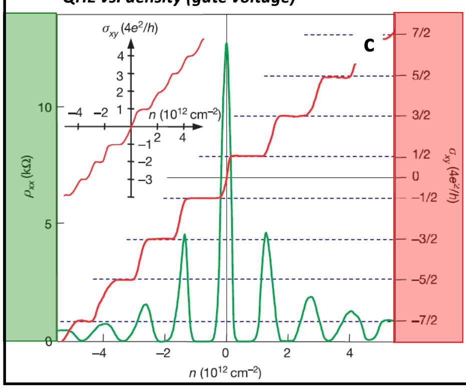

-In magnetic field Shubnikov-de Haas oscillations are presented. (b) At large B field, ρ_{xx} gets zero as for QHE.
- Great advantage of graphene, that the charge density (n) can be varied by gate voltage. QHE effect can be studied as a function of n.
-Figure c: QHE measurement at 14T, 4K.

Half-Integer Quantum Hall effect

Properties:
- Height of the Hall plateaus is $4e^2/h$
- First e (h) plateau is at $2e^2/h$
- ρ_{xx} is zero at the place of the plateaus.

$$\sigma_{xy} = 4e^2/h(n+1/2)$$

(Inset: same for multilayer graphite. The first plateau has the same height as the rest)

ρ_{xx} has maximum at n=0 → There is Landau level at zero energy. Electrons or holes contribute?

Half Integer Quantum Hall effect in graphene

Solution of the graphene Hamiltonian in B field

Let us start with the effective Dirac Hamiltonian at the K point

$$H = v\begin{pmatrix} & \pi^+ \\ \pi & \end{pmatrix}, \qquad \pi = p_x + ip_y, \quad \pi^+ = p_x - ip_y.$$

Hint: Besides a constant π and $\pi^+$are the same operators as the raising and lowering operators of the harmonic oscillator Hamiltonian of the normal 2DEG in B field, i.e. $\hat{H} = \hbar\omega_c\left(\hat{a}^+\hat{a} + \frac{1}{2}\right)$.

In case of magnetic field: $\vec{p} = \frac{\hbar}{i}\vec{\nabla} - \frac{e}{c}\vec{\mathrm{A}}, \quad \vec{\nabla} \times \vec{A} = B\overrightarrow{e_z}$

Let us use a gauge of $\vec{A} = (-By, 0, 0)$:

$$\pi = \tfrac{\hbar}{i}\partial_x + \tfrac{e}{c}By + \hbar\partial_y,$$
$$\pi^+ = \tfrac{\hbar}{i}\partial_x + \tfrac{e}{c}By - \hbar\partial_y.$$

Take the wave function ansatz, $\Psi(\vec{r}) = \begin{pmatrix} c_1\phi_n \\ c_2\phi_{n+1} \end{pmatrix}\frac{e^{ik_x x}}{\sqrt{L}}$:

$$\pi = \hbar k_x + \tfrac{e}{c}By + \hbar\partial_y,$$
$$\pi^+ = \hbar k_x + \tfrac{e}{c}By - \hbar\partial_y.$$

Replacing y by y', where $\hbar k_x + \frac{e}{c}By = \frac{e}{c}By'$:

$$\pi = \tfrac{e}{c}By' + \hbar\partial_{y'},$$
$$\pi^+ = \tfrac{e}{c}By' - \hbar\partial_{y'}.$$

N.Peres et al., PRB 73, 125411 (2006)

Half Integer Quantum Hall effect in graphene

Solution of the graphene Hamiltonian in B field

Let us introduce a^+, a which fulfills the algebra of the raising and lowering operators of the harmonic oscillator: $a = \pi^+ \frac{c}{eB}\frac{1}{\sqrt{2}r_c}$, $a^+ = \pi\frac{c}{eB}\frac{1}{\sqrt{2}r_c}$, where r_c is the cyclotron radius $r_c{}^2 = \frac{\hbar c}{eB}$.

It gives

$$a = \frac{1}{\sqrt{2}r_c}\left(y' + r_c{}^2\partial_{y'}\right),$$
$$a^+ = \frac{1}{\sqrt{2}r_c}\left(y' - r_c{}^2\partial_{y'}\right).$$

These two operators fulfill: $[a, a^+] = 1$.

ϕ_n is the eigenfunction of the a related harmonic oscillator, i.e.

$$a|\phi_n\rangle = \sqrt{n}|\phi_{n-1}\rangle, \quad a^+|\phi_n\rangle = \sqrt{n+1}|\phi_{n+1}\rangle.$$

Returning to the Dirac Hamiltonian:

$$H = v\begin{pmatrix} & \pi^+ \\ \pi & \end{pmatrix} = -v\left(\frac{c}{eB}\frac{1}{\sqrt{2}r_c}\right)^{-1}\begin{pmatrix} & a \\ a^+ & \end{pmatrix} = -v\frac{\sqrt{2}\hbar}{r_c}\begin{pmatrix} & a \\ a^+ & \end{pmatrix}$$

N.Peres et al., PRB 73, 125411 (2006)

Half Integer Quantum Hall effect in graphene

Solution of the Hamiltonian of Dirac electrons in B field

Let us start with the wavefunction $\Psi_n(\vec{r}) = \begin{pmatrix} \phi_n \\ \alpha\phi_{n+1} \end{pmatrix} \frac{e^{ik_x x}}{\sqrt{L}}$ where $\alpha = \pm 1$.

$$H\Psi_n \rightarrow \begin{pmatrix} & a \\ a^+ & \end{pmatrix} \begin{pmatrix} \phi_n \\ \alpha\phi_{n+1} \end{pmatrix} = \begin{pmatrix} \sqrt{n+1}\alpha\phi_n \\ \sqrt{n+1}\,\phi_{n+1} \end{pmatrix} = \sqrt{n+1}\alpha \begin{pmatrix} \phi_n \\ \alpha\phi_{n+1} \end{pmatrix}$$

$$H\Psi_n = -v\frac{\sqrt{2}\hbar}{r_c}\sqrt{n+1}\alpha\Psi_n$$

Landau levels in graphene: $E_n = \pm v\frac{\sqrt{2}\hbar}{r_c}\sqrt{n+1}$, $n = 0, 1, 2, \ldots$

There is an extra solution as well: $\Psi_0 = \begin{pmatrix} 0 \\ \phi_0 \end{pmatrix} \frac{e^{ik_x x}}{\sqrt{L}}$. $\quad H\Psi_0 = \begin{pmatrix} 0 \\ 0 \end{pmatrix} = E\Psi_0 \rightarrow E_0 = 0.$

Degeneracy of the levels:

Similar to normal Landau Levels. $L > y > 0 \rightarrow L > \frac{\hbar c}{eB}k_x > 0$ and $k_x = \frac{2\pi}{L}n$ where n is integer.

→The degeneracy: $N = \frac{L^2 B/c}{h/e}$ i.e. number of flux quantum penetrating the sample.

Solving the problem for the K' effective Hamiltonian gives the same spectrum as the one for K. Therefore each E_n energy level has a degeneracy of $N * 2 * 2$. 2 from the two valleys, 2 from the real spin of the electrons.

N.Peres et al., PRB 73, 125411 (2006)

Density of states

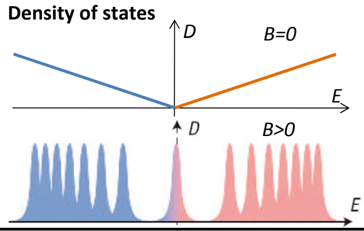

Élállapotok

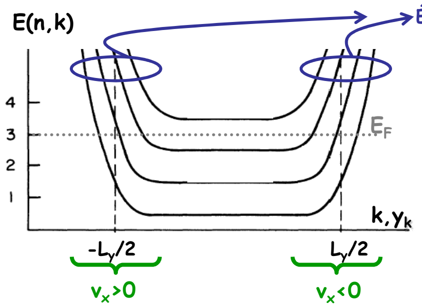

→**Élállapotok (edge states)**: a minta szélén lokalizált állapotok

Elektron állapotok x irányú sebessége:

$$v_x(n,k) = \frac{1}{\hbar}\frac{\partial E(n,k)}{\partial k} = \frac{1}{\hbar}\frac{\partial E_S(y)}{\partial y}\frac{\partial y_k}{\partial k} = \frac{1}{eB}\frac{\partial E_S(y_k)}{\partial y_k}$$

→ a minta belsejében $v_x(n,k) = 0$

→ az él állapotokra $v_x(n,k) \neq 0$, a minta két szélén az elektronok ellentétes irányba haladnak

Az élállapotoknak a minta falán pattogva előre haladó klasszikus elektron mozgás felel meg, (a minta belsejében lévő e állapotoknak körpályát leíró e mozgás feleltethető meg)

Belső e állapotok és élállapotok klasszikus megfelelői

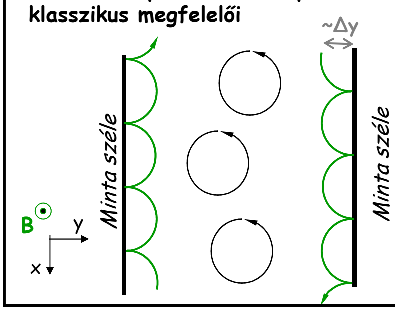

Mivel $L_y \gg \Delta y$ ($\Delta y \sim 25\text{nm}/B[\text{T}]^{0.5}$) → a mintában a **jobbra és balra haladó állapotok térben** (y irányban) **szeparálódnak**.

Ha E_F két LL között helyezkedik el, akkor csak a minta szélén vannak e-k a Fermi-felületen → Szennyezők nem képesek az e-t az egyik irányba haladó élállapotból a másik irányba haladóba átszórni →

Nincs visszaszórás

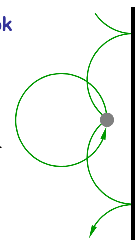

Élállapot szóródása szennyezőn

Élállapotok árama

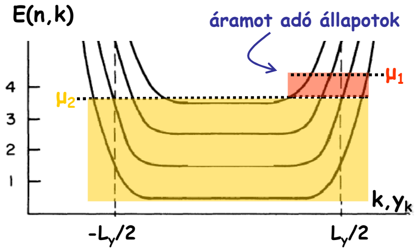

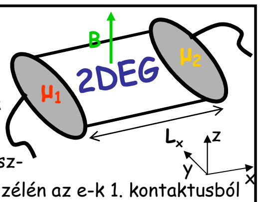

Visszaszórás hiányában a minta szélei úgy viselkednek, mint tökéletes transzmissziójú ballisztikus vezetők. A minta $y=L_y/2$ szélén az e-k 1. kontaktusból jöttek, így μ_1 lesz a kémiai potenciáljuk, míg az $y=-L_y/2$ szélén lévő állapotok 2. kontaktussal lesznek egyensúlyban.

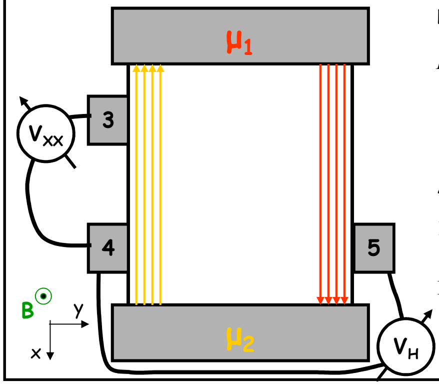

Ha V feszültséget kapcsolunk a mintára → $\mu_1-\mu_2 = eV$ ($eV<\hbar\omega$, μ_1 és μ_2 ugyanazon két LL között van)→ a μ_1 és μ_2 közötti élállapotok nettó áramot eredményeznek:

$$I=\frac{2e}{L_x}\sum_{n,k}\frac{1}{\hbar}\frac{\partial\varepsilon}{\partial k}=\frac{2e}{L_x}\sum_n\int_{\mu_2}^{\mu_1}\frac{L_x}{2\pi}\frac{1}{\hbar}\frac{\partial\varepsilon}{\partial k}dk=$$

$$=\frac{2e}{h}\sum_n\int_{\mu_2}^{\mu_1}d\varepsilon=\frac{2e}{h}M(\mu_1-\mu_2)$$, ahol M a E_F alatti LL száma.

Az ebből négypont és Hall-ellenállások:

$$R_{XX}=\frac{V_{XX}}{I}=\frac{V_4-V_3}{I}=\frac{\mu_4-\mu_3}{eI}=\frac{\mu_2-\mu_2}{eI}=0$$

$$R_H=\frac{V_H}{I}=\frac{V_5-V_4}{I}=\frac{\mu_5-\mu_4}{eI}=\frac{\mu_1-\mu_2}{eI}=\frac{h}{e^2}\cdot\frac{1}{2M}$$

→ Visszaszórás nélkül vezető élállapotok felelősek a Kvantum Hall-effektusért

Half Integer Quantum Hall effect in graphene

Solution of the Hamiltonian of Dirac electrons in B field

Remark:

The edge states behave similar to the ones of QHE of normal 2DEGs.

$$v_x=\frac{1}{\hbar}\frac{\partial E}{\partial k_x}=\frac{1}{\hbar}\frac{\partial E}{\partial y}\frac{\partial y}{\partial k_x}=\frac{1}{\hbar}\frac{\partial E}{\partial y}\frac{1}{eB/c}$$

On the two sides of the sample they propagate to opposite direction.

Half-integer quantum Hall-effect:

Due to the 2 spin and 2 valley, there are 4-fold degenerate Landau levels. Each degeneracy provides a conductance channel with $G=\frac{e^2}{h}$. Therefore each filled LL enhance the Hall conductance by $G=\frac{2\cdot 2\cdot e^2}{h}$. When E_F is placed on a LL, the Hall conductance changes from a quantized plateau to the next one. Since there is a LL at ZERO ENERGY the first electron like Hall plateau is at $G=\frac{2\cdot e^2}{h}$ and the rest are at $G=\frac{2\cdot 2\cdot e^2}{h}(n+\frac{1}{2})$.

The zero energy LL makes the QHE of graphene special. It consist e and hole states as well.

Charge density of Landau levels

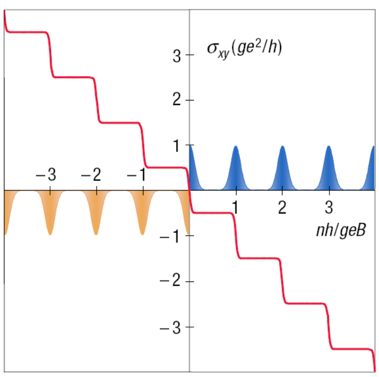

N.Peres et al., PRB 73, 125411 (2006)

Quantum Hall effect at room temperature

Landau-levels

$E_n = \pm\sqrt{2e\hbar v^2|n|B}$ 2D Dirac fermions (m=0)

$E_n = \hbar\omega_C(n+1/2)$ 2D free electrons

Comparing to GaAs based 2DEGs

Graphene:	GaAs/AlGaAs:
$E_1(B=1T)\approx 350K$	$\hbar\omega(B=1T)\approx 20K$
$E_1(B=10T)\approx 10^3K$	$\hbar\omega(B=10T)\approx 200K$
$\mu\approx 10^4$ cm²/Vs (2006) @4K	$\mu\approx 10^5$ cm²/Vs (1980)
$\mu\approx 10^6$ cm²/Vs (2010) @4K	$\mu\approx 10^7$ cm²/Vs (2004)

Experiment

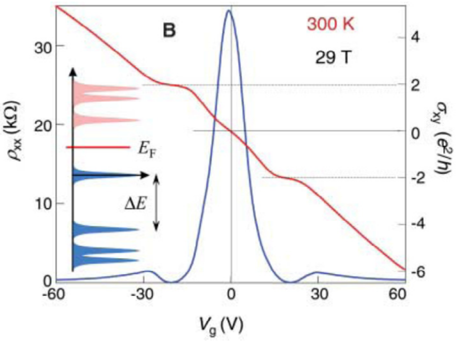

Novoselov, Science **315**, 1379 (2007)

$E_1(29T)\approx 1800K$ >>kT

$\mu\approx 10^4$ cm²/Vs @RT (weak T dependence)

Limitation of B, that $\omega_C\tau$>>1 (τ elastic mean free path).

If the amount of scattering can be further decreased, QHE gets visible at lower B fields.

→ New possibilities for current standard, quantum circuits at room temperature

Mobility and scattering mechanisms

$$E(\vec{k}) = \hbar v_F|\vec{k}|$$

Conductance in simple Drude picture:

$$\sigma = e^2\tau\frac{n}{m}$$

However the effective mass depends on k, thus one has to average 1/m for all filled states.

Accurate calculation of σ, from Boltzmann equation (see Solyom 24.3.39.):

$$\sigma = e^2\tau\frac{n}{m} = e^2\tau\cdot 2\cdot 2\cdot\int_{filled\ k\ states}\frac{d^2k}{(2\pi)^2}\frac{1}{m_{xx}}$$

Result: $\sigma = e^2\tau\frac{v_F}{\hbar\pi}k_F$

with relaxation length $l \equiv v_F\tau$

$$\sigma = \frac{2e^2}{h}lk_F$$

Mean free path: $l = \frac{\hbar}{e}\mu\sqrt{n\pi}$

E.g. for mobility =600.000, l is ≈ 3µm

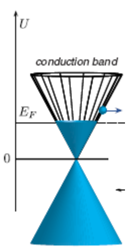

***R* vs. *V_g* Transport characteristics**

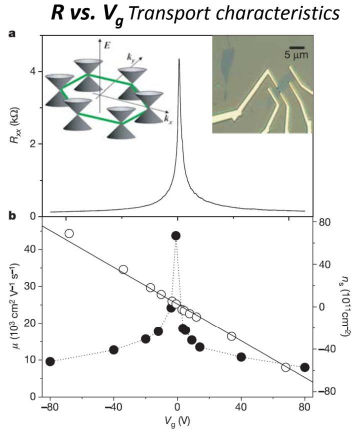

Nature 438, 201 (2005)

Mobility and scattering mechanisms

What limits the mobility at room T?

Source of 1/τ ?

Graphene on SiO_2 substrate, UHV
T=[20K-500K], 4-point

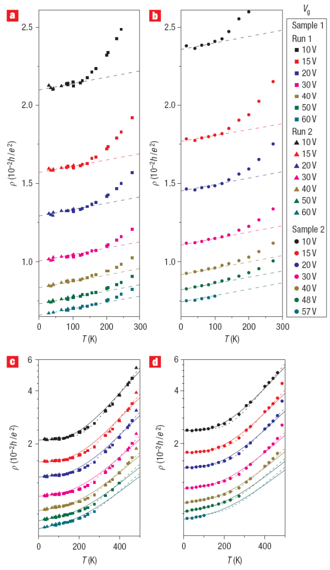

Scattering mechanisms resulting resistivity:
- potential scattering: impurities, defects, vacancies
- Electron – phonon scattering
- Etc.

Usual terms: (see Solyom II.)
- Residual resistivity (ρ_0): T independent
- Longitudinal acoustic phonons (ρ_A): linear in T

$$\rho(V_g, T) = \rho_0(V_g) + \rho_A(T); \quad \rho_A(T) = \left(\frac{h}{e^2}\right)\frac{\pi^2 D_A^2 k_B T}{2h^2 \rho_s v_s^2 v_F^2}$$

Measurements (see Fig. a,b)
- At higher T, strong deviation from linear T dependence
- Dependence also on Vg

→It suggests scattering on high energy phonon modes

Chen Nature Nanotech. 3, 206, (2008)

Mobility and scattering mechanisms

$$\rho(V_g, T) = \rho_0(V_g) + \rho_A(T) + \rho_B(V_g, T);$$
$$\rho_B(V_g, T) = B_1 V_g^{-\alpha_1}\left(\frac{1}{e^{(59\text{meV})/k_B T} - 1} + \frac{6.5}{e^{(155\text{meV})/k_B T} - 1}\right)$$

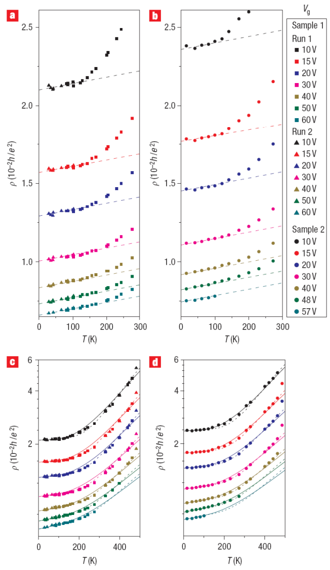

ρ_B: additional term to fit the measurements (see Fig. c,d)
Bose-Einstein distribution ~ population of high energy phonon modes, e.g. optical phonons
Very good fit of the measured curves with alfa=1.04

Optical phonons of graphene?
- Strong Vg dependence is not expected
- Mainly out of plane phonons at this energy. It is not expected to give strong contribution

Interfacial phonon scattering: Surface optical phonon modes in SiO_2 couples to e-s in graphene
The expected phonon energies and coupling strength (1:6.5) are inserted into $\boldsymbol{\rho_B}$
Strong Vg dependence is also expected

Mobility and scattering mechanisms

What limits the mobility at room T?

Different T dependence of ρ_0, ρ_A , ρ_B allows to separate the three contributions. ($\rho_B = \rho - \rho_0 - \rho_A$)

Fig. a

ρ_A V_g independent

$\rho_B \sim V_g^{-1.04}$ relation confirmed

→ **Residual resistivity dominates**

Fig. b

Derive the mobility related to two e-p processes :

$\mu = 1/ne\rho = 1/c_g V_g e\,\rho$

→ SiO_2 contribution (b) dominates

→ **The intrinsic, LA phonon scattering mobility** at $n = 10^{12}\mathrm{cm}^{-2}$ (technologically relevant) : $\mu \approx 200\,000$ (see blue dot) **Higher than any known semiconductor!** (E.g. InSb ≈77 000 and carbon nanotubes ≈100 000).

Contributions at Room T

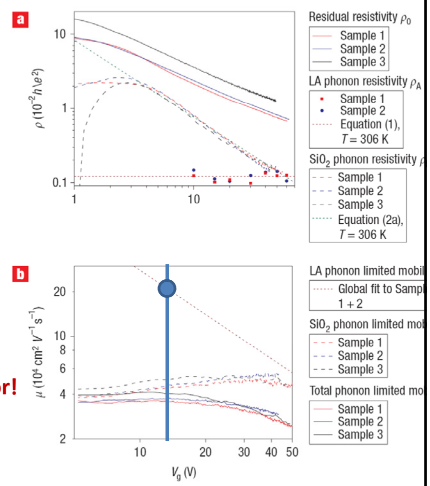

Mobility and scattering mechanisms

What limits the mobility at room T?

Different T dependence of ρ_0, ρ_A , ρ_B allows to separate the three contributions. ($\rho_B = \rho - \rho_0 - \rho_A$)

Fig. a

ρ_A V_g independent

$\rho_B \sim V_g^{\,i-1.04}$ relation confirmed

→ **Residual resistivity dominates**

Fig. b

Derive the mobility related to two e-p processes :

$\mu = 1/ne\rho = 1/c_g V_g e\,\rho$

→ SiO_2 contribution (c) dominates

→ **The intrinsic, LA phonon scattering mobility** at $n = 10^{12}\mathrm{cm}^{-2}$ (technologically relevant) : $\mu \approx 200\,000$ (see blue line) **Higher than any known semiconductor!** (E.g. InSb ≈77 000 and carbon nanotubes ≈100 000).

T dependence

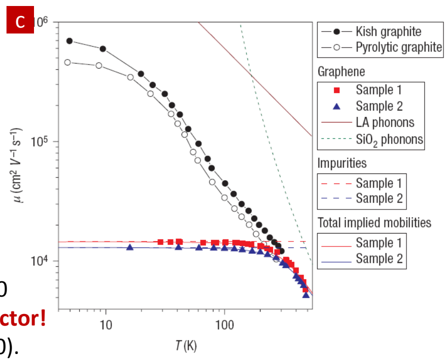

Fig. c

Comparision with graphites, sources of exfoliated graphene

Mobility is much smaller than for graphites. It is impurity dominated.

→Residual res. not due to point defects but due to **charge impurities in SiO_2 substrate**

Σ: Problem, SiO_2 is bad substrate

Suspended flakes

To improve mobility eliminate the substrate. → Suspended graphene samples
Two techniques:

- Etched SiO by BHF

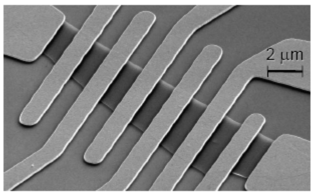

low-T mobilities: few million cm²/V·s
This high quality samples allowed to demonstrate Fractional QHE in graphene

At room T the mobility is 10k- 100k cm²/V·s ?
New flexural phonons appears in suspended samples, low energy out of plane vibrations
→ Try to apply tension

Andrei, Kim & Yacoby also Manchester

- Use an organic polimer bellow, expose and desolve

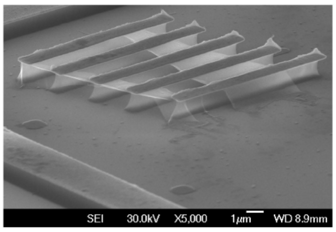

PMGI based organic polymer
Possible with any metal contacts! →
spin physics, superconductivity
600.000 cm2/Vs @5.0 E9 cm^{-2},77K. L~3μm
→Observation of
condcutance quantization,
0.7 anomaly

N. Tombros arXiv:1009.4213

Suspended flakes

Conductance quantization in graphene
- PMGI based organic polimer
- short and wide channels, reduce the role of edge roughness
- K-K' valley degeneracy is lifted.

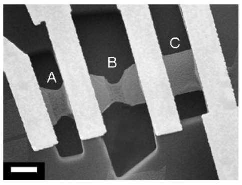

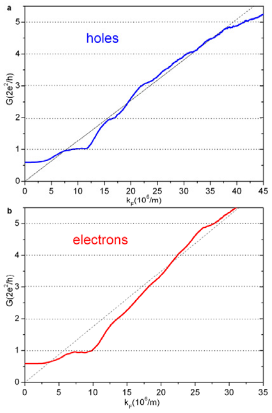

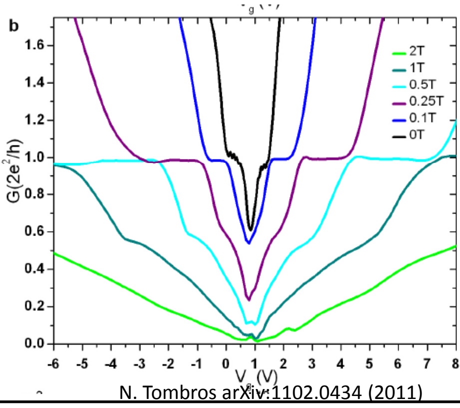

N. Tombros arXiv:1102.0434 (2011)

Better substrate – Boronnitride

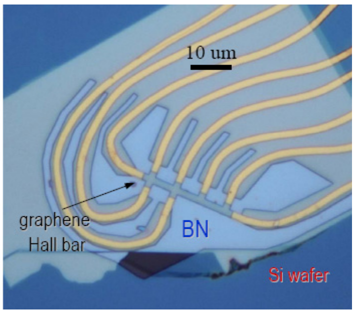

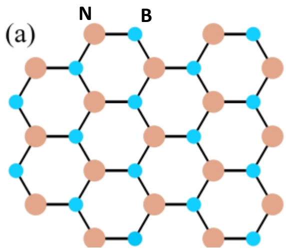

room-T mobility
close to 100,000 cm2/V·s

Advantages:
- Atomically smooth surface that is relatively free of dangling bonds and charge traps.
- Lattice constant similar to that of graphite, and has large optical phonon modes and a large electrical bandgap.

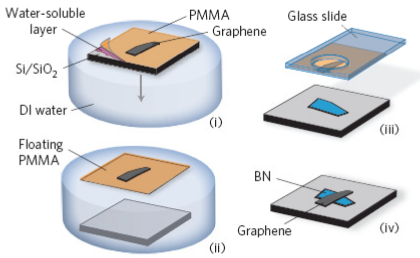

Dean et. al., NatureNanotech 5, 722 (2010)

Carbon Nanostructures

II. Carbon Nanotubes (CNT)

Outline:

- Single walled carbon nanotubes (wrapping)
- Synthesis
- Electronic properties (metallic vs. semiconducting CNT)
- Quantum transport (Ballistic conductance, Fabry-Perot interference)
- CNT Quantum dots (spin, orbital degeneracy, Orbital and SU(4) Kondo effect)

References:

- S Ilani and P. L. McEuen Annu. Rev. Condens. Matter Phys 1, 1–25 2010. and references within.
- P. Jarillo-Herrero, Quantum transport in carbon nanotubes, phd thesis 2005.
- Wikipedia: en.wikipedia.org/wiki/Carbon_nanotubes

Carbon Nanotubes (CNT)

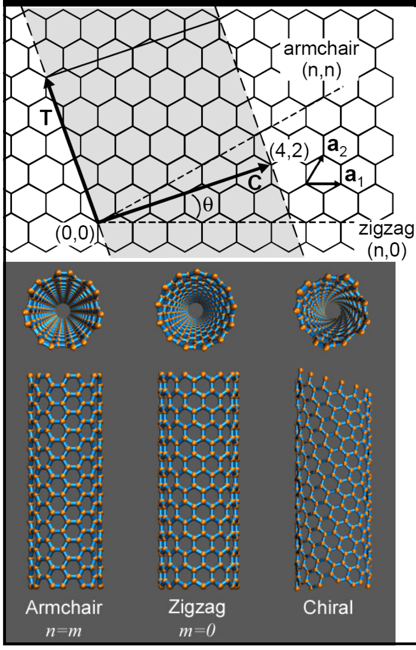

CNT = Big carbon molecule, Rolled up graphene with half buckyballs at the ends.
Diameter ~nm, length up to 15cm
Single-walled CNT
Multi-walled CNT

Single walled nanotubes:
Band gap 0-2eV, semiconductor or metallic
Wrapping vector (n,m) : determines the waist of the CNT
C= na_1+ma_2
Special CNT, which are not chiral:
- Zigzag CNT: m=0:
- Armchair CNT: m=n

Synthesis of CNT

Nanotube
1D

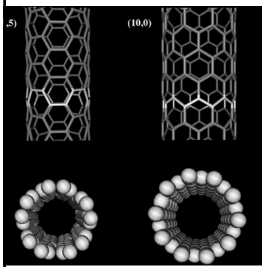

1991
S Iijima
Electron microscope

- **Arc discharge** (original method)
graphite electrode + voltage,
30% of weight could generate CNT
- **Laser ablation**
pulzed laser on graphite target in inert gas.
CNT are forming on cold surface yield of 70%, mainly single wall
- **CVD (Chemical vapor deposition)**
Metal catalyst particle (Ni, Fe) on the surface, high T (700C) and carbon containing gases (e.g. acetylane)
Advantage: Possible to grow directly on the surface

Big challenge: controlled growth only certain chirality, or large scale separation
90-95% selection of semiconducting or metallic SWCNT is possible

Similar good mechanic, heat conducting and electric properties as for graphene

Electronic properties of CNT

Band structure

Metallic or semiconducting?

Starting point is the band structure of graphene (a).
Rolling up → periodic boundary condition i.e. quantization of the e wavenumber in the circum-ferencial direction, $k_\perp$:

$$\Delta k_\perp \pi d = 2\pi,$$

where d is the diameter of the tube.
→1D bands form from discrete slices of the graphene spectrum

If a slice passes through the Dirac point (see Fig. c) → Metallic CNT
If not → Semiconducting CNT (see Fig.b)

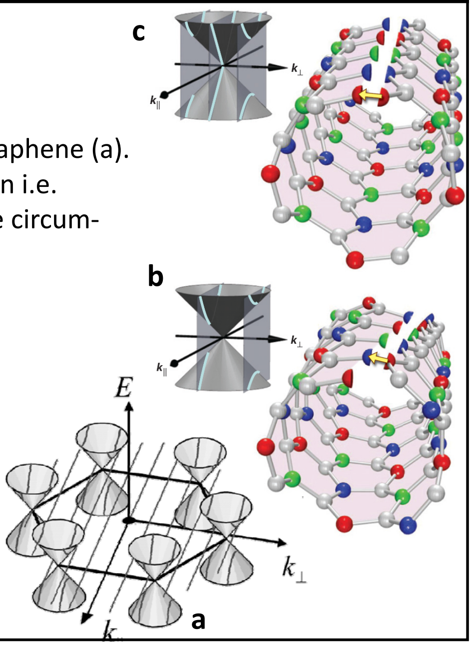

Electronic properties of CNT

Fig. d: phase of K point wavefunction of graphene. Due to 3-fold symmetry A atoms have three possible phases: 0, 120°, 240°, color coded by red, green, blue.

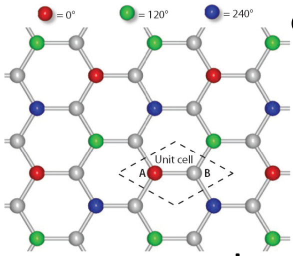

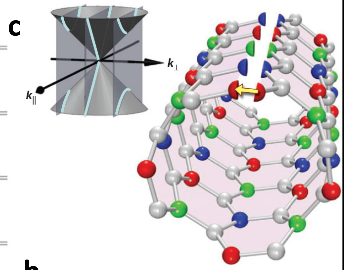

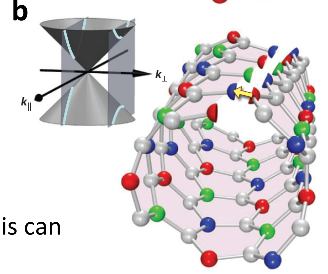

There are two ways of rolling up:
- Red atom rolled to an other red one (Fig. c).

→Wave function satisfies the boundary condition i.e. wave function in K is a legitimate solution on the cylinder. → There is slice pass through K → metallic CNT (Fig. c) (MCNT)

-Red atom rolled to blue or green (Fig. b)

There is a phase mismatch of 2/3π at the boundaries. This can be solved by changing K to $K+k^0_\perp$, where $k^0_\perp \pi d=-2/3\,\pi$

→ lowest quantized wavefunction is away from K → semiconducting CNT (Fig. b) (SCNT)

Consequences: - 2/3 of CNTs are semiconducting
- with energy gap of $E_g = 2\cdot\hbar v_F k^0_\perp = 4\,\hbar v_F/3d \approx 0.7\,eV/d[nm]$

Electronic properties of CNT

In reality usual metallic tubes also shows **small bandgap**. Since the metallic band structure is instable against perturbation like e.g. mechanical deformation. Everything what destroys A⇔B symmetry (i.e. pseudospin) generates gap. Taken into account the curvature of small diameter CNTs also generates gap.

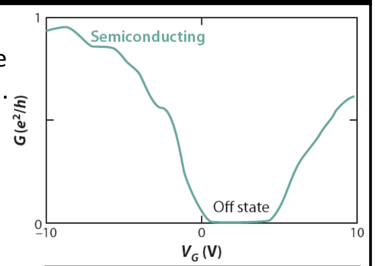

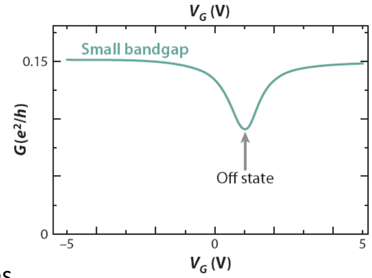

Figures: measured transport characteristics @RT. Gate electrode is used to change the e filling.

Maximal conductance:

In Landauer picture each ballistic subband gives a maximal conductance of e^2/h. In CNT there are 4 subbands, due to 2 spin and 2 isospin (valley K, K') degeneracies. I.e. $G_{max}=4e^2/h$.

The conductance is also limited by contact resistances. It has to be a clear transparent barrier. For semiconductor tubes palladium gives Schottky-barrier free contacts for p-type CNTs. While Al with low work function gives good contact to n-type CNTs.

Electronic properties of CNT

Typical numbers of mean free path and mobility:
l_e ~100nm (SCNT) ~1µm (MCNT) @RoomT and
µ>100.000 cm²/Vs (SCNT), l_e ~10µm (MCNT) @<50K

The large mean free path has the same origin as for graphene. C has light mass, sp² is a strong bonds → high energy phonons, which are only populated at high T.

Limit of maximal current
At large source drain biases, e-s accelerate in the tube and can excite optical zone boundary phonons. This dramatically decrease l_e to 10nm, and thereby this voltage threshold limits the current:

$$I_{max} \sim 4e^2/h\ \hbar\omega_0/e \sim 25\mu A$$

$\hbar\omega_0 = 160$meV.

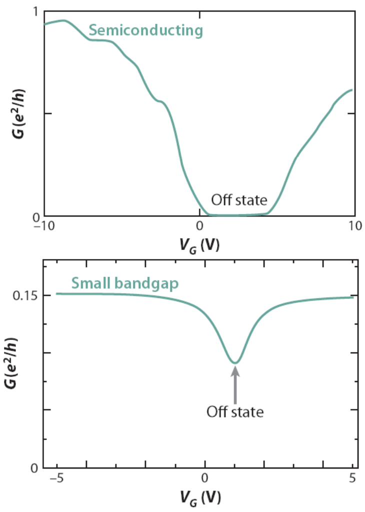

Quantum transport of CNT

Ballistic and coherent transport at low T (T<5K)

Fabry-Perot cavity
Due to coherent scattering on the imperfect contacts interferences occur: periodic oscillations as a function of gate and bias. V_g or bias changes k and thereby the accumulated phase on one loop.
Periodicity (V_c) is proportional to L^{-1}, where L is the length of CNT segment.

Sample geometry with electron path scattered on the contact interfaces

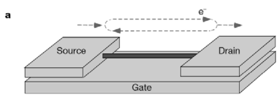

Corresponding scattering matrix problem

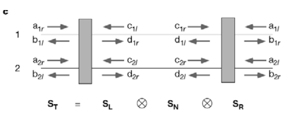

Periodicity of the oscillations vs. Length of the CNT segment
periodicity determined by arrow position in right figure

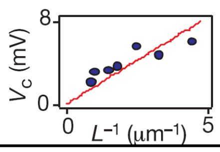

G vs. V_g and Bias

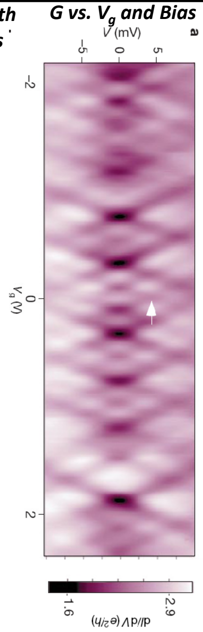

CNT Quantum dots

Quantum dots:
If the barrier resistance R~h/e^2, e-s are localized between the contacts.
→ Qdot physics.
Typical charging energy:

$$U \approx 5\text{–}20\ \mathrm{meV}/L[\mu m]$$

For short segments also large level spacing, transport through individual quantum levels.

Dispersion relation of CNT

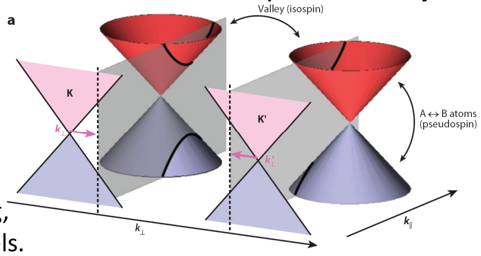

Shell structure:
Graphene has three 2-fold symmetries:
Pseudo spin A⇔B, Isospin (K, K'), electron spin
First generates the Dirac spectrum (e-h symmetry)
Second two induce 4-fold degenerate levels of Qdot with SU(4)

Level spectrum and symmetries of CNT QDot

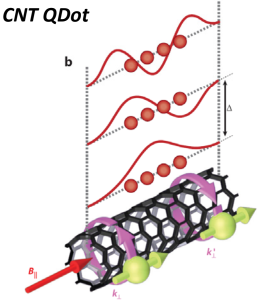

The K'/ K isospin corresponds to solution encircle clockwise /anticlockwise around the tube. From valley degeneracy of graphene → orbital degeneracy of Qdot levels.
In a Qdot longitudinal momentum is also quantized: $\Delta k_{||} = \pi/L$
resulting a level spacing of: $\Delta = \hbar v_F \Delta k_{||}$

CNT Quantum dots

Experiments:
The 4-fold degenerate shells were observed in experiments. Every 4th Coulomb diamond is wider. Level spacing has to be paid when a new shell opens. If there is disorder the isospin degeneracy is lifted. (see right lowest Fig.) Mostly this is the case, only newest ultraclean CNT devices show 4-fold degeneracy.

Qdot levels demonstrating the shells with 4 levels

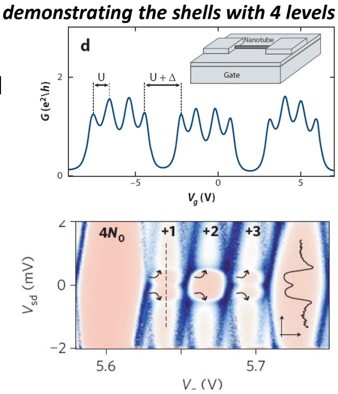

The 4 states in the shell can be split by applying B field parallel to tube axis:

$$E^{\uparrow/\downarrow}_{CW/CCW} = -(\mu_{orb} + \mu_{spin})\cdot B_{||} = \left(\pm\frac{dev_F}{4} \pm \tfrac{1}{2} g\mu_B\right) B_{||}$$

B field dependence of the 4 levels

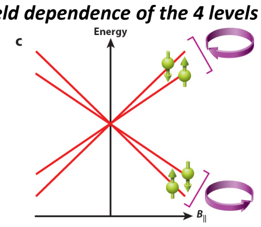

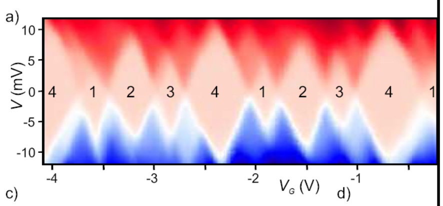

c) d)

Jespersen NaturePhys10.1038 (2011) & Physical Review B 71, 153402 (2005).

CNT Quantum dots

In semiconducting CNTs one can access the single electron and single hole filling of the quantum dot (see right figs). Large diamond corresponds to the empty quantum dot.

In ultraclean CNTs (grown on top of the electrodes) shell structure was studied at single e filling (see bottom left fig.).

1e and 1 hole state of semiconducting CNTs

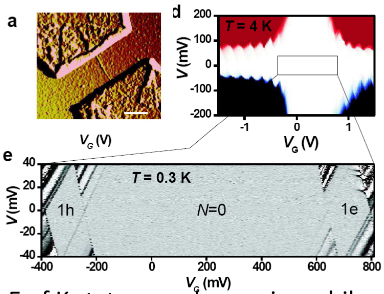

***Evolution of the 4 states in B field** V_{sd}=-2mV*

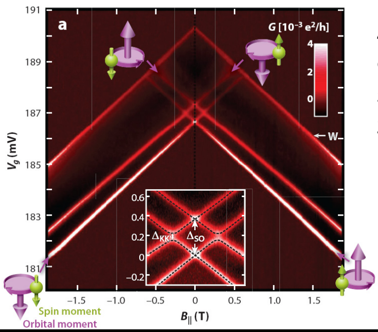

As B|| increased E of K states are decreasing while one of K' increasing, similar to figure on previous slide.

Surprising that at B=0 the four states are split in two 2-fold degenerate levels. See also inset for zoom in.

Reason: **spin orbit coupling**. E-s on K and K' orbitals induce B field, which effects the e spin

$$B_{SO} = -(\mathbf{v} \times \mathbf{E})/c^2$$

→ K↓ and K`↑ get lower energy. SU(4) symmetry is lifted.

Nature 429, 389 (2004).

SU(4) and orbital Kondo effect in CNT

Kondo situations in CNT Qdot:

a) Normal Kondo: Two degenerated spin states
b) Orbital Kondo: Two orbitals have the same energy
c) Two orbitals x two spin states are degenerate

Kondo situations in CNT

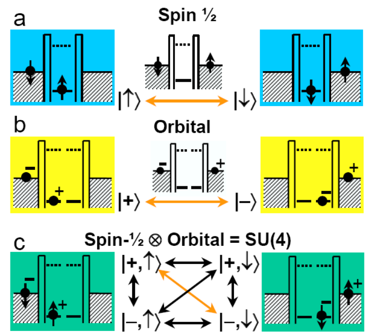

Yellow region: at finite B field two states with same spin get degenerate, inducing a situation of orbital Kondo effect

Green region: 4-fould degeneracy, spin and orbital induces a SU(2)xSU(2)=SU(4) Kondo situation

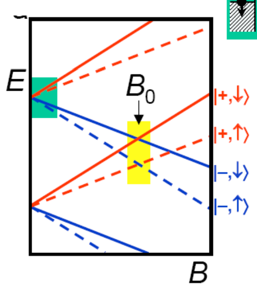

P Jarillo-Herrero Nature 434,484 (2005)

SU(4) and orbital Kondo effect in CNT

Orbital Kondo effect

Fig. a) At B=5.8T for 1e occupation of the last shell (I) there is a conductance increase due to Kondo effect, see yellow dotted line. (Orange numbers are the spin of the dot, green lines are boarder between charge states)

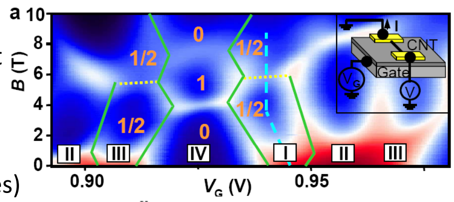

Fig. b) Bias slice at the Orbital Kondo situation (B=5.9T, V_g=937mV). Inset: Peak height follows Kondo scaling.

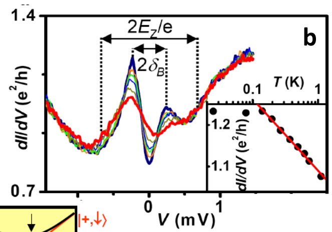

Yellow region: at finite B field two states with same spin get degenerate, inducing a situation of orbital Kondo effect

Green region: 4-fould degeneracy, spin and orbital induces a SU(2)xSU(2)=SU(4) Kondo situation

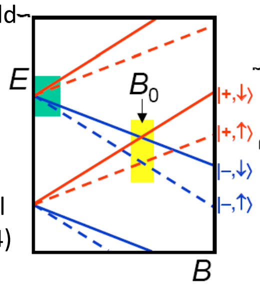

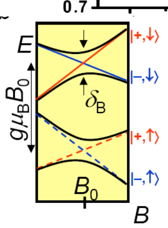

Zoom in of yellow region: anticrossing δ_B due to coupling between |+> and |->

P Jarillo-Herrero Nature 434,484 (2005)

SU(4) and orbital Kondo effect in CNT

SU(4) Kondo effect signatures

Fig. a) Decreasing T, G increases in the valley of state I and III.

Fig. b) B=0 zero bias resonance appears in state I and III. (There is no orbital splitting as in previous slide due to higher Kondo temperature $\delta_B < T_K$)

Fig. c) At B=1.5T the Kondo resonance splits into 4 branches for state I

Fig. d) The splitting of the 4 states vs. B field for state I.

Outer lines are cotunneling from |-> to |+> orbitals, while the inner lines are cotunneling process from |-,↑> to |-,↓>. ($\mu_{spin}=\mu_B$, $\mu_{orbital}$ = 13μ_B)

The multiple splitting provides direct evidence of the SU(4) Kondo resonance.

(For B=1.5T & III the inner two states are not split. Since T_k large spin-1/2 SU(2) Kondo remains.)

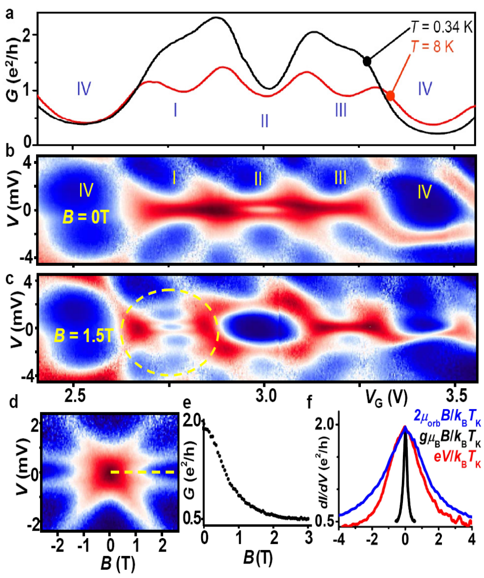

P Jarillo-Herrero Nature 434,484 (2005)